Cannibalism Shapes Biofilm Structure and Composition in *Bacillus subtilis*

Lena Friebel[1], Jan-Philipp Knepper[3], Nathalie Sofie Becker[1,2], Gorkhmaz Abbaszade[4], Kathrin Stückrath[4], Susann Müller[4], Klaus Dreisewerd[3], and Thorsten Mascher[1*]

[1] TUD University of Technology Dresden, Chair of General Microbiology, Dresden, Germany
[2] University of Tübingen, Interfaculty Institute of Microbiology and Infection Medicine, Tübingen, Germany
[3] University of Münster, Institute of Hygiene, Münster, Germany
[4] Helmholtz Centre for Environmental Research-UFZ, Department of Applied Microbial Ecology, Leipzig, Germany

---

Abstract

Bacillus subtilis can form robust colony biofilms in which different phenotypic subpopulations co-exist in highly structured and complex multicellular communities with tissue-like properties. These subpopulations provide the colony with an overall competitive fitness and the ability to respond to everchanging environmental conditions. But biofilms also provide a structural framework for both colony expansion and long-term survival in the form of highly resilient endospores. In this context, cannibalism is thought to delay sporulation by enabling one subpopulation of cells, the cannibals, to produce the sporulation delay protein SDP, the sporulation killing factor SKF and the epipeptide EPE. These cannibalism toxins lyse susceptible non-producers, thereby releasing nutrients to prevent premature sporulation. Here, we comprehensively characterized a collection of mutants defective in either toxin production or the corresponding autoimmunity by combining luminescence reporters, colony biopsy, multi-parameter flow cytometry and MALDI-mass spectrometry imaging to resolve cannibalism function and distribution. Our findings demonstrate that EPE and SDP are critical in delaying sporulation, while SKF does not significantly influence spore abundance. The three toxins are produced in distinct, only partially overlapping areas of the colony and interdepend in their spatial distribution. The absence of all three toxins (ΔΔΔ mutant) led to hyper-sporulation and small colonies characterized by excessive wrinkle formation, indicating that cannibalism-driven cell death is essential for maintaining biofilm structure and lateral expansion. Furthermore, the loss of autoimmunity against EPE and SDP resulted in severe morphological changes and stress-induced occurrence of suppressor mutants, thereby underscoring the importance of toxin resistance mechanisms. Our results highlight the complex interplay between the three cannibalism toxins, which together influence the spatiotemporal organisation, morphology and subpopulation dynamics within *B. subtilis* biofilms. By integrating different methodologies, we provide the first evidence of the complex interactions that shape biofilm architecture through bacterial programmed cell death mediated by localized toxin production and spatial distribution.

Introduction

Biofilms as a collective mode of bacterial life appeared over three billion years ago on our planet (De la Fuente-Núñez et al., 2013). The ability to form these structured, multicellular aggregates likely evolved as a survival strategy in response to the harsh environmental conditions of early Earth. This evolutionary step allowed bacterial cells to thrive and survive in a self-produced, matrix-protected, and surface-adherent microenvironment, in which collective behaviors and differentiated multicellular traits could develop (Flemming et al., 2021).

The soil-dwelling, Gram-positive bacterium *Bacillus subtilis* is a model organism for studying (multi)cellular differentiation and development in complex biofilms. This bacterium possesses the remarkable ability to transition from a motile to a sessile lifestyle, in which it forms dormant endospores within the context of differentiated biofilms (Branda et al., 2001). *B. subtilis* can form different types of biofilms, depending on the respective environment: pellicle biofilms at the liquid-air interface, colony biofilms at the solid-air interface, and submerged surface-attached biofilms (Arnaouteli et al., 2021). Within *B. subtilis* biofilms, different cell types emerge in a spatiotemporally controlled manner during differentiation in response to specific microenvironments, e.g., based on the availability of nutrients (Yannarell et al., 2023). These processes are guided by appropriate, tightly regulated gene expression programs, but also influenced by stochastic gene expression and genetic noise (Y. Chai et al., 2008; Chu et al., 2006; Lopez et al., 2009; Milton & Cavanagh, 2023). A key player of genetic regulation is the master regulator of sporulation, Spo0A, which orchestrates cell differentiation once external stimuli propose harsh living conditions that favor the formation of endospores (Fujita et al., 2005; Hamon & Lazazzera, 2001; Molle et al., 2003; Rahman et al., 2021). Spo0A becomes activated through a multicomponent phosphorelay, resulting in increasing levels of Spo0A~P over time (Burbulys et al., 1991; Trach et al., 1991). As a consequence, it gradually silences regulatory repression of its counterplayer, the transition state regulator AbrB, which suppresses premature activation of stationary phase traits: increasing cellular Spo0A~P levels repress the expression of *abrB* (M. Strauch et al., 1990a). Low levels of Spo0A~P trigger the differentiation of cells into producing the extracellular matrix (ECM), essential for biofilm formation (Fujita et al., 2005; Shafikhani et al., 2002). This subpopulation then displays elevated levels of matrix-associated genes, in a SinR-dependent manner (Newman et al., 2013). The extracellular matrix comprises exopolysaccharides, amyloid TasA fibers, and the hydrophobin-like protein BslA, which forms a hydrophobic biofilm coating (Arnaouteli et al., 2021). Interestingly, matrix-producing cells also exhibit characteristics of cannibalistic cells (López et al., 2009).

Cannibalism is a social behavior in *B. subtilis* that occurs in the early sporulation phase, that is, at low Spo0A~P levels (González-Pastor, 2011). A subset of cells is thought to produce cannibalism toxins that will lyse neighboring non-cannibalistic cells to release nutrients, which then may help delaying commitment to sporulation in the cannibalistic cells. Cannibalism is determined by expressing the operons encoding the sporulation killing factor SKF, the sporulation

delaying protein SDP, and the more recently discovered epipeptide EPE (Fujita et al., 2005; González-Pastor et al., 2003; Popp et al., 2020).

The *skfABCEFGH* operon contains the structural gene for the SKF toxin (*skfA*), genes for the toxin maturation machinery (*skfB*, *skfC*), an ATP-binding cassette (ABC) transporter that mediates autoimmunity to SKF (*skfEF*), as well as two genes of yet unknown function (*skfG*, *skfH*) (González-Pastor et al., 2003; Höfler et al., 2016a). The *sdpABC-sdpIR* locus consists of the toxin-encoding gene *sdpC*; the gene products of *sdpA* and *sdpB* are required for toxin maturation, while *sdpIR* encodes the autoimmunity, with SdpR being a transcriptional repressor and SdpI an SDP-sequestering lipoprotein (Ellermeier et al., 2006). Within the *epeXEPAB* operon, *epeX* encodes the prepropeptide for a secreted antimicrobial peptide (EPE), *epeE* encodes a radical S-adenosyl-L-methionine (SAM) epimerase, which is necessary for maturation and processing of the EPE toxin, together with the transmembrane peptidase, encoded by *epeP*. The genes *epeAB* encode an ABC transporter that mediates autoimmunity against intrinsically produced EPE (Popp et al., 2020). These toxins, classified as ribosomally synthesized and post-translationally modified peptides (RiPPs), disrupt cell membrane integrity. While the exact mode of action of SKF remains unclear, SDP and EPE have been extensively studied. SDP collapses the proton motive force and triggers autolysis (Lamsa et al., 2012), while EPE dissipates membrane potential, reduces membrane fluidity, and induces lipid domain formation (Popp et al., 2020). As a consequence of producing these destructive molecules, *B. subtilis* mounts a defense strategy known as the cell envelope stress response (CESR) (Jordan et al., 2008; Radeck et al., 2017). EPE primarily activates the two-component system LiaRS, which upregulates the *liaIH* operon to confer resistance against extrinsically applied EPE (Popp et al., 2021). BceRS and PsdRS respond to SDP and primarily SKF (Höfler et al., 2016). Both two-component systems regulate ABC transporters, BceAB and PsdAB respectively, which provide resistance against antimicrobial peptides (Staroń et al., 2011).

Cannibalism is a bacterial form of programmed cell death (PCD) (Popp & Mascher, 2019). It plays a pivotal role in structuring bacterial colonies by facilitating wrinkle formation (Asally et al., 2012). These wrinkles result from vertical buckling movements driven by localized cell death, alleviating the mechanical stress associated with high cell densities and rapid cell division. Wrinkle formation depends on surface adhesion and extracellular matrix production, as matrix-deficient mutants fail to develop these structural features (Romero et al., 2014). These interconnected wrinkles enhance biofilm function by creating nutrient- and waste-transporting channels, and improving overall biofilm physiology (Chai et al., 2024; Wang et al., 2016). While the biophysical processes of biofilm formation have been addressed in recent years, very little is known about the relationship between structural organization and differentiation processes, such as cannibalism, which remains largely unexplored. This knowledge gap is the consequence of the technological challenges in studying bacterial multicellular aggregates due to the size restrictions. Understanding the interdependence of the multicellular 'form' and the emerging 'functions' of

bacterial biofilms requires resolving macroscopic structure, such as colony biofilms, at (near to) single cell resolution. But recent breakthroughs in instrumentation and imaging technology now allow implementing multiscale, high-resolution approaches to be utilized for studying differentiated microbial communities (Espinoza Miranda et al., 2025). These approaches allow gaining insights into the complex structural organization of biofilms and help identifying subpopulations, and even the function of individual cells within such structures and subpopulations.

In this study, we investigated the role of cannibalism in the spatial and temporal organization of *B. subtilis* colony biofilms. By combining multiparameter flow cytometry and imaging mass spectrometry with genetic alterations, we analyzed the distribution and dynamics of cannibalism toxins and the resulting distribution of different cell types within biofilms. This approach allowed us to elucidate how cannibalism-induced PCD contributes to biofilm architecture and the resulting emerging multicellular function.

Results

Cannibalism affects the morphology of *B. subtilis* colony biofilms

Cannibalism is a differentiation strategy that involves sacrificing one subpopulation for the benefit of another, which only makes sense in the context of multicellular populations. In addition to cell death, cannibalism was previously associated with matrix production and hence biofilm formation (López et al., 2009). But despite this clear connection, cannibalism has so far not been studied in the context of differentiated bacterial tissue. We therefore initially investigated whether cannibalism mutants of *Bacillus subtilis* derived from the undomesticated, transformable strain 3A38 exhibited altered morphologies in colony architecture compared to the otherwise isogenic wild type strain 3A38 (hereafter referred to as WT). Colony morphology was examined by cultivating strains of interest on agar plates of the biofilm-promoting minimal medium MSgg (minimal salts glycerol glutamate) at 28°C and monitoring biofilm formation over eight days, by capturing daily images (Fig. 1). Cannibalistic mutants were either defective in toxin production due to deletions of the structural genes that encodes the pre-pro-peptide (*epeX*, *sdpC*, *skfA*), or lacked the autoimmunity functions to the respective toxins (*epeAB*, *sdpI*, *skfEF*). Additionally, we investigated a strain lacking all three cannibalistic toxin-encoding loci (Δ*epeXEPAB* Δ*sdpABCRI* Δ*skfABCEFGH*, abbreviated as ΔΔΔ, and referred to as the hypo-cannibalistic mutant).

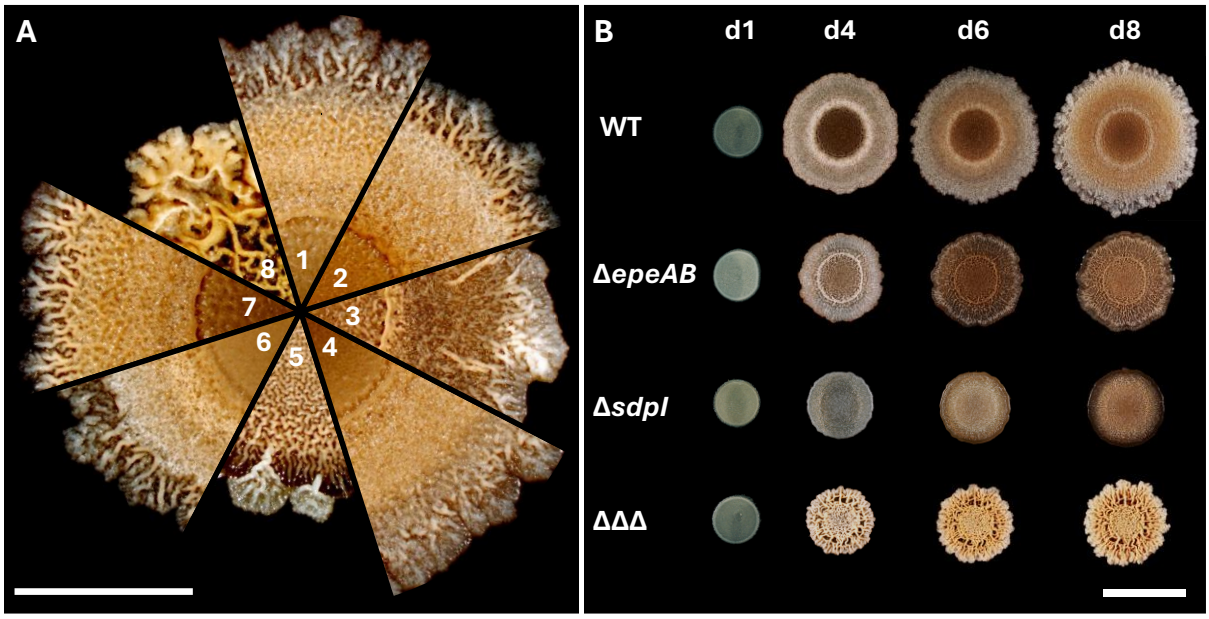

Fig. 1 **Colony morphologies of *B. subtilis* cannibalistic mutant strains in comparison to the WT.** [A] Comparative display of 8 day old biofilms grown on MSgg agar. 1-WT, 2-Δ*epeX,* 3-Δ*epeAB,* 4-Δ*sdpC,* 5-Δ*sdpI,* 6-Δ*skfA,* 7-Δ*skfEF,* 8-ΔΔΔ. Scale bar indicates 0.5cm. [B] Colony growth and morphology of cannibalistic mutants with distinct phenotypes (Δ*epeAB,* Δ*sdpI*, ΔΔΔ) in comparison to WT over the course of 8 days (day 1 [d1], day 4 [d4], day 6 [d6], day 8 [d8]). Scale bar indicates 1cm.

The WT formed a circular biofilm with an undulating edge, characterized by vein-like, intertwined, brownish three-dimensional (3D) structures, in agreement with previous descriptions (Branda et al., 2001). The colony exhibited three distinct zones: (i) the center, marking the inoculation site, separated by a ring-like structure from (ii) the inner zone, which was beige in color, primarily flat,

but slightly elevated toward (iii) the outer zone. The outer zone was highly structured, featuring pronounced wrinkles extending to the colony's edge, with a more brownish-grey hue compared to the other zones.

Deletion of *epeX*, *sdpC*, or *skfA* had only minor effects on colony morphology, like a rather reddish tint across colonies of the *epeX* mutant. The *sdpC* mutant exhibited reduced wrinkle formation in the outer zone, resulting in a flatter, broader surface. Morphological differences in other mutants became apparent from day four onward (Fig. 1B). Deletion of the autoimmunity genes for EPE (Δ*epeAB*) or SDP (Δ*sdpI*) led to pronounced changes in colony size, color, and structure. In contrast, Δ*skfEF* exhibited no major effects and retained a WT-like colony appearance (Fig. 1, Fig. S1). Notably, the *sdpI* (autoimmunity) mutant displayed convoluted structures resembling human brain folds (Fig. 1A-5), with an indistinct boundary between the inner and outer zone. Here, the outer zone appeared in a darker brown with reduced structuring. The *epeAB* mutant also showed a color shift toward brown across the entire colony, though all three zones remained distinguishable. Both, Δ*epeAB* and Δ*sdpI* biofilms exhibited sporadic white outgrowths in the outer zone, appearing to "escape" from the colony, a phenomenon described further in Fig. 4. The most striking colony architecture occurred in the hypo-cannibalistic mutant (ΔΔΔ). Its biofilm is characterized by a highly wrinkled surface featuring a structurally complex, folded region surrounding the center. The colony displayed increased vertical growth with reduced lateral expansion. Compared to the WT's beige wrinkles, those of ΔΔΔ were more yellowish, broader, and less defined toward the periphery. In summary, while SKF did not affect the colony structure, the absence of SDP or EPE autoimmunity or – and most pronounced – the complete loss of cannibalistic features (ΔΔΔ) led to significant alterations in colony structure, size, and pigmentation. Cannibalism toxins are therefore an important determinant of colony structure, differentiation and expansion.

<u>Cannibalism toxins show unique and interdependent distribution patterns</u>

Based on these structural consequences on colony architecture as described above, we next explored whether specific structural alterations could be correlated with the presence or absence of the three cannibalism toxins within the biofilm. Towards that end, we applied matrix-assisted laser desorption ionization mass spectrometry imaging (MALDI-MSI) (Brockmann et al., 2019) to visualize the distribution of mature EPE (17 amino acids (aa)), SDP (42 aa), and SKF (26 aa) with a spatial resolution of about 50 µm pixel size. Whole biofilms were grown on 150 µm thick mixed cellulose ester membranes and, following a brief fixation step for inactivation (except for WT strains), were spray-coated with 2,5-dihydroxyacetophenon MALDI matrix (see Materials and Methods for details). A hybrid time-of-flight (QTOF) mass spectrometer (timsTOF fleX MALDI-2, Bruker Daltonics, Bremen, Germany) was employed to register the MALDI-generated ion traces. MALDI-MSI is a label-free technique that registers all generated ions simultaneously within a mass acquisition range based on their specific mass-to-charge (m/z) values – which in turn are

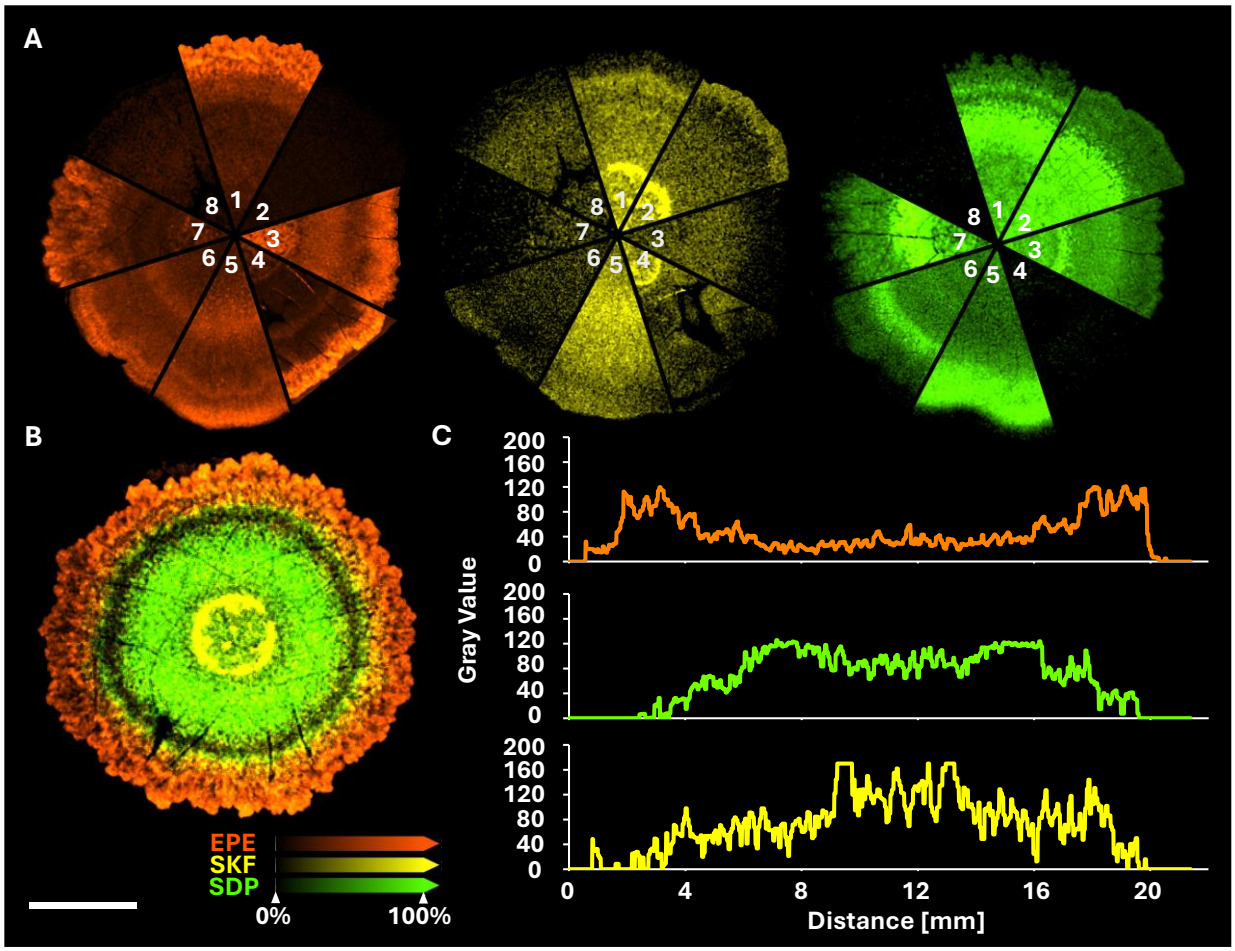

***Fig. 2* Overlay MALDI-MS images of cannibalistic toxins EPE, SDP and SKF in wild type and mutant *B. subtilis* biofilms.** [A] Representative slices of the biofilm covering center, inner and outer zone, displaying the distribution of EPE, SKF, and SDP (from left to right) in the WT (1) and cannibalistic mutant strains (2-Δ*epeX,* 3-Δ*epeAB,* 4-Δ*sdpC,* 5-Δ*sdpI,* 6-Δ*skfA,* 7-Δ*skfEF,* 8-ΔΔΔ). [B] Distribution of EPE, SKF and SDP across the whole colony of the WT. Scale bar indicates 0.5 cm. [C] 2D-plot of toxin distribution across the distance of the biofilm conducted by linear pixel intensity measurement (gray pixel values). Plateaus at approx. 9-9.7 mm and 12.9-13.2 mm indicate a maximal gray value of 170 in SKF measurement.

defined by the molecular composition and type of charge-providing adduct ion. In our case, the m/z values of interest were the following: EPE was recorded most prominently at m/z values of 2108.09 and 2146.04 presenting the monoisotopic $[M + H]^+$ and $[M + K]^+$ ions, respectively; SDP at m/z 4314.22 ($[M + H]^+$) and 4352.18 ($[M + K]^+$), and SKF at m/z 2783.31 ($[M + H]^+$) and 2821.27 ($[M + K]^+$). An example mass spectrum is depicted in Fig. S3. False-color images are used to illustrate the registration (and ultimately occurrence within laser-probed sampling pixel in a semi-quantitative fashion) of the three cannibalism toxins across mature eight day old biofilms of the WT and all cannibalistic mutants strains. In general, all the investigated *B. subtilis* biofilms that were investigated exhibited radial symmetry with regard to their morphologies and peptide toxin production. We therefore combined slices from biofilm pictures of each of the eight strains into one scheme (Fig. 2). EPE (depicted in orange color) is predominantly located in the outer zone of the colony (Fig. 2A-1, 2B, 2C). As expected, no EPE signal was detected in the *epeX* deletion strain (Fig. 2A-2) or the hypo-cannibalistic mutant (Fig. 2A-8). The distinct distribution of EPE was

lost in the *skfA* mutant, which is unable to produce SKF (Fig. 2A-6) but slightly accentuated in the *sdpC* mutant, where SDP is absent (Fig. 2A-4). The MALDI-MSI data suggest that SKF is particularly enriched in the border between region between the central and inner zone of the WT biofilm, forming a distinct ring that correlates well with colony morphology. In the absence of EPE (Fig. 2A-2), SKF was “redistributed” to the outer zone, where EPE was “originally” located in the WT. The absence of EPE and SDP-autoimmunity (Fig. 2A-3/5, respectively) resulted in the loss of the characteristic SKF ring in the colony center, leaving a weak and broad distribution pattern across the remaining biofilm. No SKF was detected in the *skfA* deletion strain or the hypo-cannibalistic mutant, confirming the absence of EPE, SDP, and SKF in this mutant. Furthermore, SKF was undetectable in the *skfEF* mutant strain (Fig. 2A-7, Fig. S3), suggesting that SKF production depends on the presence of its respective autoimmunity factors. Such a connection between autoimmunity and production has so far not been observed and is a unique feature of SKF that stands in contrast to SDP and EPE. While the false-color images indicate a weak signal throughout the biofilm, the corresponding mass spectra revealed that these base signals represent noise rather than the presence of SKF (Fig. 2A-6/7/8, Fig. S3).

In the WT biofilm, SDP (depicted in green color) was primarily located in the inner zone (Fig. 2A- 1). However, its distribution is significantly altered in strains lacking the autoimmunity genes for EPE (Δ*epeAB*, Fig. 2A-3) or SDP (Δ*sdpI*, Fig. 2A-5), as well as in the absence of SKF. Within the biofilm of the *epeAB* mutant, SDP strongly accumulated at the central ring structure, whereas in a *sdpI* mutant biofilm, SDP is predominantly found in the outer zone. In the *skfA* mutant, SDP localizes strongly at the border between the inner and outer zone of the biofilm. Interestingly, the distribution of SDP in a *skfEF* mutant is comparable to the WT, even though we demonstrated that no SKF is in this mutant. Hence, this effect might depend on SkfEF function rather than SKF itself. As anticipated, SDP was not detected in the *sdpC* deletion and the hypo-cannibalistic mutant.

The combined picture on the distribution of the three toxins in the WT strain reveals that they collectively cover the entire colony area, each with its own preferred zone (Fig. 2B): A quantitative analysis of the gray pixel values in the WT biofilm was conducted by linear pixel intensity measurement (Fig. 2C). Concurrent with the afore described MALDI-MSI results, EPE predominantly covers the outer zone, SDP is the inner zone, and SKF peaks in the center of the colony, although it is also lightly present in other zones. This suggests a distributional interdependence among the three toxins that requires further investigation.

Expression of *epeX* correlates with EPE production

We had previously demonstrated that cannibalism toxins intrinsically trigger the CESR (Höfler et al., 2016; Popp & Mascher, 2019). P_{lial}, P_{bceA}, and P_{psdA}, when fused to the *luxABCDE* reporter cassette, provide a highly specific, cannibalism-induced luminescent readout, with P_{lial} responding to EPE-stress, while P_{bceA}/P_{psdA} were triggered by both SDP and particularly by SKF, at least in liquid cultures of strains derived from the domesticated laboratory reference strain W168. We therefore wondered whether these reporters could also be applied for recording cannibalism stress during colony development in undomesticated strains We therefore measured the spatiotemporal distribution of toxin gene expression (P_{epeX}, P_{sdpA}, and P_{skfA} for EPE, SDP and SKF, respectively) and the corresponding CESR in developing biofilms over the course of eight days. Promoter activities were examined in WT biofilms and in autoimmunity-deficient strains for all three toxins. For SKF and SDP the results obtain for W168-derived reporters in liquid culture could not be reproduced neither for colonies of 3A38-derived strains.

We therefore focused on the two promoters associated with EPE-related stress (Fig. 3). The promoter driving *epeX* expression, P_{epeX}, exhibited strong activity throughout the whole developmental period, with a prominent signal observed in the outer zone of the biofilm,

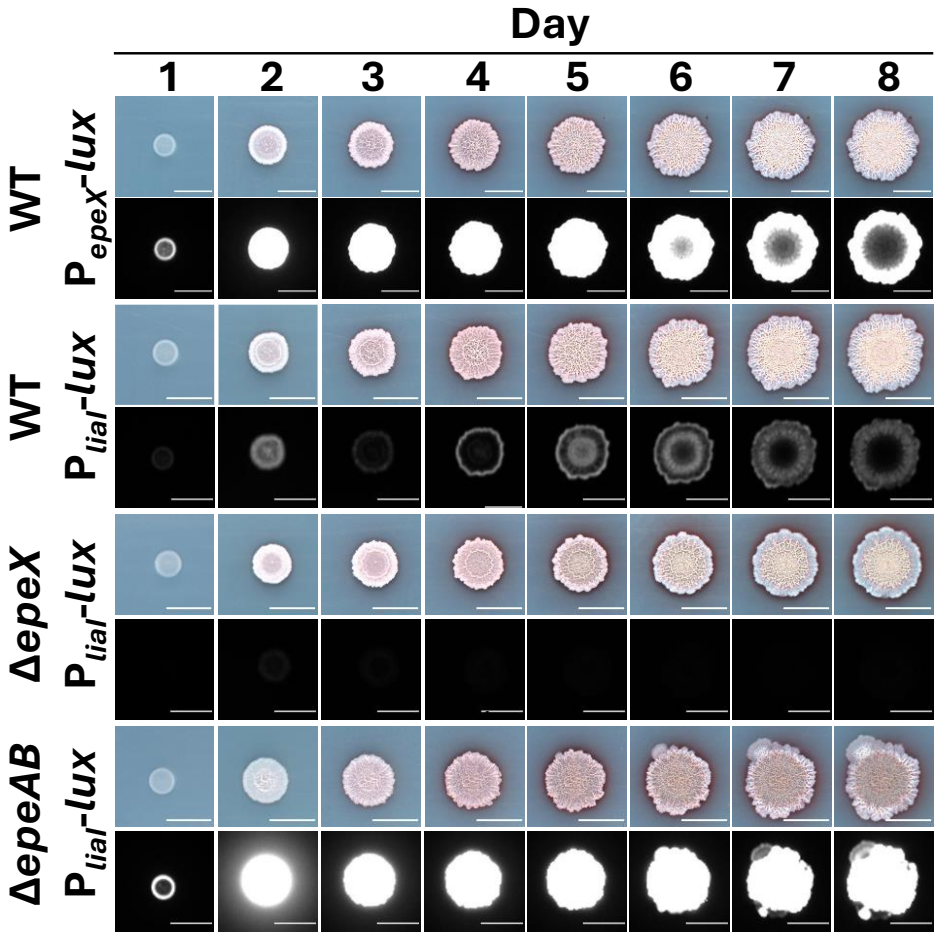

Fig. 3 **Activity of promoters of *epeX* and the corresponding stress response *lial*** fused to a *luxABCDE*-cassette in WT and mutant strains on MSgg agar. Colony expansion and luminescence signal distribution are shown over the course of 8 days. Scale bar indicates 1 cm.

resembling the inoculation spot, already on day 1 (24 hours post-inoculation). From day 2 to day 5, the signal spread across the entire colony. From day 6 onwards, activity steadily decreased from center of the colony, so that by day 8, P_{epeX} activity was confined to the outer zone. The corresponding EPE stress-responsive promoter, P_{lial}, revealed an intriguing ring pattern during biofilm growth. But from the third day onwards, the P_{lial} signal is predominantly located at the edge of the biofilm and – particularly towards the end of colony differentiation, the activity of P_{epeX} and P_{lial} co-localize (days 7-8). The distribution of the P_{lial}-*lux* signal indicates that while the *epeXEPAB* locus is consistently expressed (P_{epeX}-*lux* readout), active EPE is not directly released. This observation indicates that maturation or release of active EPE are tightly regulated beyond the transcriptional control of P_{epeX}. Importantly, the P_{lial}-*lux* readout at the end of colony development perfectly overlaps with the location of mature EPE toxin, as detected by mass spec imaging (Fig. 2).

Since P_{lial}-*lux* seemed indeed suitable as a readout for EPE release, we next probed following P_{lial} activity in an EPE-OFF strain (Δ*epeX*). The absence of any P_{lial} activity in this strain corroborates that the Lia system indeed specifically responds to EPE stress in differentiating colonies. In contrast, the massively increased P_{lial}-*lux* signal in the autoimmunity mutant (Δ*epeAB*) demonstrates that EpeAB indeed counteracts EPE stress in colony biofilms. Without this ABC transporter, P_{lial} activity was persistently strong and spread across the entire colony, resembling the pattern seen in the WT for P_{epeX}.

<u>EPE stress in autoimmunity mutants gives rise to suppressor mutants</u>

Interestingly, from day 7 onward, only weak P_{lial} activity was detected in specific areas of the colony edge, indicating a reduction in EPE stress due to decreased EPE production. Moreover, these “flares” remained white, suggesting a lack of sporulation. In fact, such outgrowths were frequently observed at the edges of biofilms from strains harboring either *epeAB* or *sdpI* deletions. When isolated, their white color and altered colony morphology remained segregationally stable (Fig. S2), indicating that these flares represent suppressor mutants that occurred under severe cannibalism stress. One of these isolated spontaneous mutants was subsequently characterized by whole-genome sequencing of genomic DNA and luminescence-based analysis of P_{epeX} and P_{lial} promoter activities in the corresponding strains. We identified a single nucleotide polymorphism (SNP) in the Spo0A binding site within the promoter region of *abrB* (Fig. 4A). Sequence analysis of the *abrB* promoter region from the other flares identified additional – but not identical – SNPs in the Spo0A consensus sequence (TGNCGAA) at genome positions 3,508,948 (G to A), 3,508,949 (T to C), 3,508,9454 (A to G), and 3,508,946 (C to T).

It is known that Spo0A binding to this promoter results in a repression of *abrB* expression (Strauch et al., 1990). Interferences with Spo0A binding should result in elevated AbrB levels and hence a repression of its target genes, thereby suppressing sporulation but also cannibalism toxin production. And this is exactly what we observed by studying the respective target promoters.

The G to A substitution in the Spo0A binding site of the *abrB* promoter identified in flare suppressor mutant 1 affected not only biofilm morphology and sporulation (Fig. 4), but also *epeX*

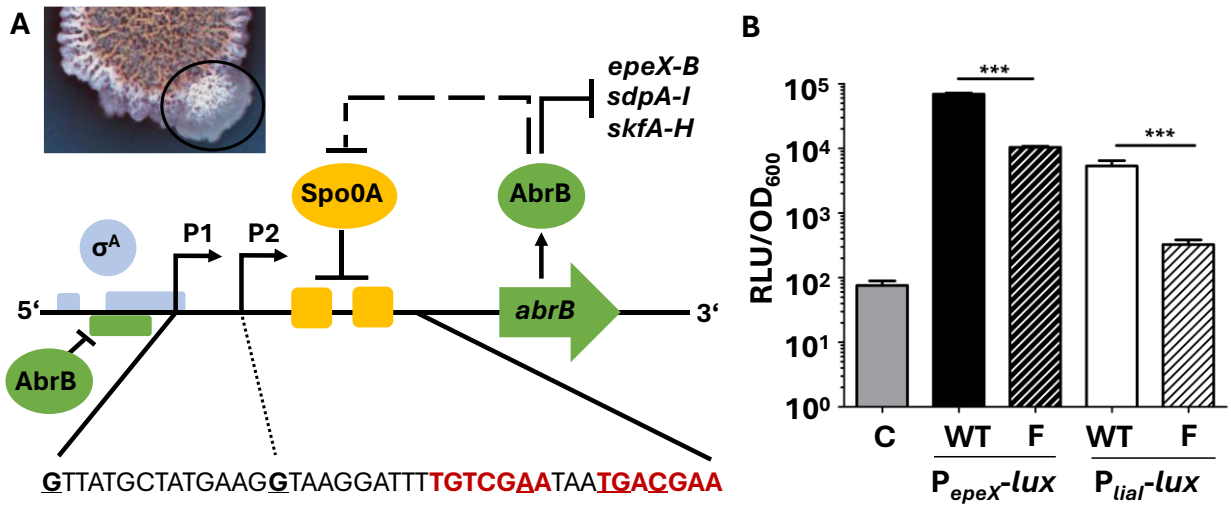

Fig. 4* Various, singularly occurring single nucleotide polymorphisms (SNPs) in the Spo0A binding sites of the *abrB* promoter region allows escape mechanism in suppressor mutants of Δ*epeAB* strains.** [A] Image of an Δ*epeAB* colony with a circle highlighting the outgrowth of a flare (suppressor mutant). Beneath, a scheme showing the location of the SNPs within the Spo0A binding sites (red underlined nucleotides) and the influence they have on the intricate interplay of Spo0A and AbrB in regard to cannibalistic operon expression. [B] Significant differences in activity of P_{epeX}-lux (black) and P_{lialI}-lux (white) in the wild type (WT) and Δ*epeAB* flares (F) showing a reduced expression of *epeX* and the corresponding stress response *lialI* in those suppressor mutants (indicate a P value <0.001) . C indicates the control (P_{empty}-*lux*).

and *sdpC* expression in a repressive manner (Fig. S2). As a consequence of the approximately 10-fold reduction in P_{epeX} activity, the corresponding EPE stress response in the flare mutants, monitored by P_{lialI} activity, was also reduced by a factor of 10 compared to the WT. This result demonstrates that the EPE- or SDP-stress is so deleterious for the biofilm population that it gives rise to suppressor mutants that interfere with the central stationary phase regulation. The transition state regulator AbrB controls over 250 genes during the transition between vegetative growth and the onset of stationary phase, including functions involved in sporulation, motility, matrix formation, quorum sensing, and cannibalism toxin production (Schultz et al., 2009; Strauch, Perego, et al., 1989; Strauch, Spiegelman, et al., 1989). De-repression of *abrB* is therefore an ideally suited strategy for escaping cannibalism stress, e.g., induced by EPE, through the suppression of toxin production based on inhibition of Spo0A binding at the *abrB* promoter.

Colony biopsy unravels cannibalism-dependent effects on cell type distribution within biofilms

The architecture of multicellular colony biofilms is characterized by a spatiotemporal controlled phenotypic diversification of different cell types – a result of the regulatory cascades governing differentiation in response to external stimuli such as nutrient and oxygen availability in combination with the underlying stochastic gene expression 'noise' (Besharova et al., 2016; Dar et al., 2021; De Kievit et al., 2001; Parsek & Tolker-Nielsen, 2008; Serra et al., 2013; van Gestel et al., 2015). Such spatial patterning has also been observed for *B. subtilis* colonies: Matrix-producing cells are located primarily in the upper layers of the biofilm, providing structural integrity through the secretion of extracellular components. Motile cells are found at the periphery, where swarming motility facilitates expansion. Sporulating cells are found in nutrient-deprived central-upper regions of the colony, which partially coincides with cannibalistic cells that delay spore formation by lysing sibling cells for further nutrient supply. Finally, competent cells, which can take up extracellular DNA to enhance genetic diversity, are dispersed heterogeneously (Branda et al., 2001; Lopez et al., 2009; Vlamakis et al., 2008). Given the observed influence of cannibalism toxins on colony architecture and their interdependent distribution patterns, we wondered whether the cell type distribution within colonies was also affected as a function of cannibalism toxin action. We therefore investigated the spatial occurrence of different cell types throughout the colony. Towards this goal, we employed colony biopsy in combination with microbial flow cytometry and cytometric fingerprinting (Abbaszade et al., 2025) on fully grown biofilms (8 days old). Biopsies were collected from six different sampling sites of the biofilm, covering zones with structural differences as well as areas with distinct toxin distributions (Fig. 5A). Each sample was then analyzed for the presence of spores, live and dead cells (Fig. 5) as well as cell cycle states, to assess population heterogeneity (Fig. S5). Both intrinsic parameters, such as scattering, and extrinsic parameters, such as fluorescence, were measured using flow cytometry. To differentiate living from dead cells, a combination of SYTO9 (a green-fluorescent, membrane-permeant nucleic acid stain) and propidium iodide (PI, which indicates compromised cell membranes and cell walls) was used for staining (Fig. 5). In addition to the SYTO9-/PI- staining, cell cycle states were assessed using 4',6-di-amidino-2-phenylindole (DAPI), a dye that intercalates into AT-rich regions of double-stranded DNA. The resulting cell subsets are displayed as 2D plots, with cell gates defined for fluorescence-activated cell sorting (FACS) (Fig. S4, Fig. S6). Based on these gates, we analyzed the changes in cell distribution between the WT and cannibalism mutant strains.

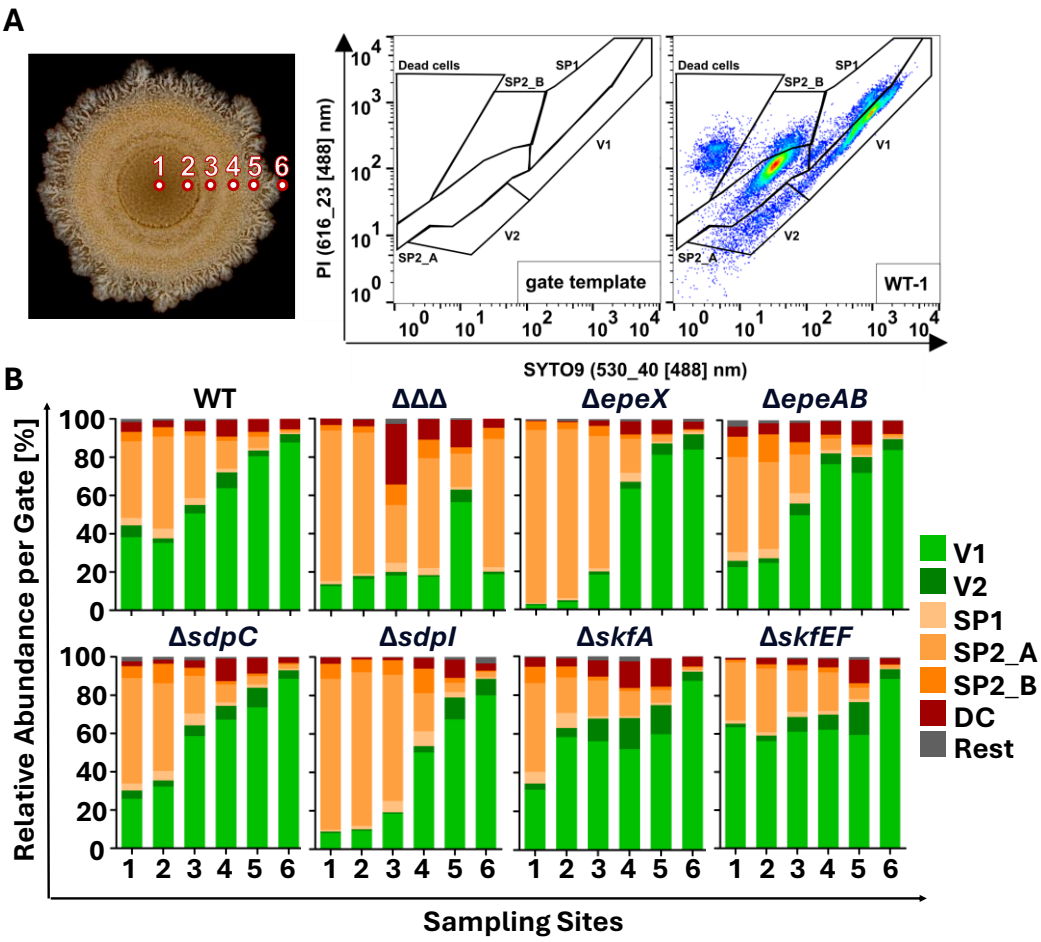

Fig. 5 **Distribution of live, dead and sporulating cells across *B. subtilis* colonies in regard to cannibalism.** [A] Sampling sites across an exemplary WT colony are shown, as well as the gate template for analysis and sorting together with an exemplary dataset of flow cytometric measurement of cells present in sampling site 1 of the WT. PI signal is plotted against SYTO9 signal. [B] Overview of flow cytometric analysis results are summarized in bar graphs for each strain, where the relative abundance of cells per gate are plotted against sampling sites. V1 and V2 indicate vegetative cells, SP1 – SP2_B represent different spore types, DC indicates dead cells.

Six distinct subpopulations could be identified within *B. subtilis* biofilms, based on SYTO9-/PI-staining: three spore types (SP1, SP2_A, SP2_B), two vegetative cell types (V1, V2), and dead cells (DC). Dead cells exhibited only red PI fluorescence, while spores showed low to medium SYTO9 fluorescence compared to vegetative cells, which appeared in the rightmost gates of the 2D plots (Fig. 5A). In the WT, a high percentage of spores were detected at sampling sites 1-3 (48.9%, 58.1%, 38.5%, respectively) (Fig. 5B, Fig. S5), located in the center and the adjacent area of the inner zone. Within the inner zone (sampling site 4), the percentage of spores decreased to 18.7%, while vegetative cells increased to 72%. This trend continued towards the outer zone (sampling sites 5 and 6), where only 2.5% of cells were spores, but 92% were vegetative cells, with a moderate 5% of dead cells. The analysis of DAPI-stained cells (Fig. S4, Fig. S6) supported this distribution , with an excess of dormant spores and sporulating cells found in the center of the colony (53.69% at sampling site 1), and the proportion of spores also decreasing towards the outer zone of the biofilm (sampling site 6).

This cell type distribution was clearly affected in most cannibalistic mutants. Specifically, the Δ*epeX*, Δ*epeAB*, and Δ*sdpI* strains showed a noteworthy increase in spore levels at sites 1-3, while Δ*sdpC*, Δ*skfA*, and Δ*skfEF* mutants displayed results like the WT. The increased spore abundance, particularly in the center and adjacent regions of the inner zone, may explain the red coloration observed in the *epeX* mutant. Previous studies have shown that sites of sporulation tend to exhibit darker biofilm coloration (Donovan et al., 1987; Hullo et al., 2001). The rise in spore numbers in toxin deletion strains is consistent with earlier observations (López et al., 2009), further supporting the hypothesis that cannibalism is a strategy to delay sporulation. Interestingly, this pattern was only observed in the *epeX* and *sdpC* mutants but not in the *skfA* mutant for both the SYTO9-PI and the DAPI-staining analyses (Fig. 5, Fig. S4).

Based on the increased CESR in autoimmunity-deficient mutants, we expected an increase in dead cells in these strains. This assumption that was not supported by the data. While approximately 5.6% of cells were dead in the WT colony, only a slight increase was observed in the *epeAB* mutant (8.4%), while the abundance of dead cells across the entire colony decreased in the *sdpI* (3.8%) and *skfEF* (4.3%) mutants.

Again, the most remarkable results came from the hypo-cannibalistic mutant, which was also most severely affected in its colony architecture (Fig. 1). Colony biopsy and flow cytometry revealed a completely rearranged distribution of vegetative, dead, and sporulating cells in comparison to the WT. In this hypo-cannibalistic mutant, spores were highly abundant across all sampling sites, even in the outer zone. The entire colony of the cannibalistic triple mutant contained 58% spores and only 34% vegetative cells, whereas the WT had 22% spores and 71% vegetative cells. Comparable results were obtained in the DAPI analyses (Fig. S4, Fig. S6). While the overall abundance of dead cells increased only slightly by 0.94% in the triple mutant compared to the WT, a closer examination of the spatial distribution of dead cells revealed significantly elevated percentages at sampling sites 3-5 (31.6%, 10.6%, 14.2%, respectively). This pattern was not observed in any of the other mutants and may offer an explanation for the highly folded structure of the colony.

Taken together, the flow cytometry results are in good agreement with the effects on colony architecture observed in the different mutant strains. The more severe the overall structure was affected, the more pronounced were the underlying changes in cell type distribution throughout the colony. This is particularly obvious in the hypo-cannibalistic mutant, which shows a complete loss of the zoning in its colony compared to the WT: The colony does not expand much beyond the area initially spotted, but instead wrinkles uniformly across its complete surface (Fig. 1). This is reflected by the even distribution of spores through the colony (Fig. 5B). The combined action of the three cannibalism toxins is crucial for both structure and function of the differentiated colonies, presumably by affecting the spatiotemporal control of colony differentiation.

Discussion

B. subtilis has evolved multiple survival strategies in response to the perpetual shifts in environmental conditions, as well as to compete with other organisms for nutrients. Differentiation in the context of multicellular aggregates such as colony biofilms gives rise to the development of different specialized cell types. This division of labor enhances the adaptability of an organism to its environment and thereby increases the chances for survival, particularly in unpredictable habitats, where change is the only constant (Qin et al., 2022). In *B. subtilis,* a complex regulatory network orchestrates and coordinates these differentiation strategies and ensures an appropriate adaptation. Under conditions of prolonged nutrient deprivation, cells of *B. subtilis* can initiate sporulation, which will ultimately result in dormant and highly resistant endospores that can outlast long periods of adverse conditions, while maintaining the ability to germinant once the conditions become more favorable again (Piggot & Hilbert, 2004). Since sporulation is an irreversible process and both time and energy-consuming, *B. subtilis* employs other survival strategies aimed at preventing are at least delaying commitment to this differentiation process.

In *B. subtilis*, cannibalism has been described as a survival mechanism that delays sporulation under nutrient-limiting conditions by enabling a subpopulation of cells to lyse their neighbors and utilize the released nutrients (González-Pastor et al., 2003). Earlier studies already demonstrated the cannibalism-dependent delay of sporulation for the undomesticated laboratory strain: in *sdp/skf* mutants, heat-resistant colony-forming units appeared earlier and in higher numbers, compared to the wild type (González-Pastor, 2011; López et al., 2009). In the present study, we could verify this function of cannibalism for the undomesticated ancestor strain and in the context of differentiated colony biofilms: the hypo-cannibalistic mutant (ΔΔΔ, Fig. 5), which is unable to produce any of the three cannibalistic toxins, showed a strong increase in spore abundance across the whole colony. In contrast to the initial studies cited above, which only considered SDP and SKF, we conclude that EPE and SDP, but not SKF, are primarily important in delaying the onset of sporulation, since the *skfA* mutant does not display a higher spore abundance compared to the WT (Fig. 5).

While delaying sporulation is therefore indeed an important function of cannibalism toxins, irrespective of different strain backgrounds and physiological settings, the mechanism by which this is achieved seems to differ between them. The originally phrased hypothesis suggested that altruistic killing of one subpopulation by another is the reason for the sporulation, due to the released nutrients (González-Pastor et al., 2003). In contrast, our current study did not provide any evidence for a cannibalism-dependent killing. Indeed, cell death seems to be primarily associated with sporulation itself, since the number of dead cells increases with the sporulation rate, but is independent of the presence or absence of cannibalism toxins (Fig. 5).

Instead of lysis, we could demonstrate for the first time a crucial role of cannibalism toxins for structuring and functionalizing colony biofilms (Fig. 1). While some indirect evidence for a link between SDP/SKF and matrix production had indicated a role of cannibalism toxin in biofilm

formation (López et al., 2009), a direct impact of cannibalism on multicellular differentiation had so far not been reported. Here, we could demonstrate that cannibalism affects both the 3D-structuring of colonies but also balance differentiation and expansion of colonies, as most prominently observed for the hypo-cannibalism strain (Fig. 1). This strain, which lacked all three cannibalism toxin loci was characterized by hyper-wrinkling, a lack of colony expansion and a massively increased sporulation rate all across the colony. This result suggests that cannibalism toxins balance colony differentiation by restricting the degree and amount of wrinkling (growth in height) and thereby ensuring that resources are provided for colony expansion (growth in width). This hypothesis would also explain the results from colony biopsy and flow cytometry. Growing in height moves a significant fraction of cells in the multicellular tissue away from the agar surface and hence away from the source of nutrients. Sporulation and cell death would be the consequences, just as we observed for the hypo-cannibalism strain (Fig. 5). In contrast, colony expansion increases the colony surface area that gets in contact with the substratum, thereby providing access to new sources for nutrients.

In the context of colony differentiation, we observed the strongest impact of individual mutations for the absence of autoimmunity in case of EPE and SDP, but not for SKF regarding both colony morphology (Fig. 1) and distribution and abundance of vegetative, sporulating and dead cell types across the colony biofilm (Fig. 5). Moreover, we observed massively increased CESR in the absence of autoimmunity, at least for EPE (Fig. 3), that seemed to provoke the generation of suppressor mutations to circumvent the stress (Fig. 4), which highlights the importance of a functional defense system towards intrinsically produced toxins. While we did not detect any increased cannibalism-dependent cell death under these circumstances, we were able to observe strongly increased stress in colonies lacking EPE autoimmunity (Fig. 3).

Our results also shed some new light on the sporulation killing factor, SKF. The eponymous killing property of SKF was so far only demonstrated in liquid cultures (López et al., 2009). Under these conditions, we also observed a strong CESR, based on the P_{psdA} and P_{bceA} biosensor read-out (Höfler et al., 2016). In contrast, we were unable to observe any inhibitory activity of SKF for colony biofilms grown on agar plates and no CESR could be detected with the same reporter strains as above. This could be attributed to either the inability to adequately enrich SKF within the plate-based assays or the explanation may be found in the distribution of the toxin in the surface-attached biofilm. Our MALDI-MS imaging experiments demonstrated that SKF is predominantly located in the center of the biofilm and to a lesser extent, at the periphery. The latter finding is consistent with an independent study demonstrating the localization of SKF at the outer boundary of the biofilm. Additionally, this study, which also employed MALDI-MS imaging, demonstrated that a *srfAC* mutant, which could no longer produce surfactin, was also deficient in SKF production (Dinesen et al., 2025). Cannibalism has previously already been associated with surfactin (López et al., 2009). Taking into account the recent findings by Dinesen and colleagues, this provokes the question of how and why this biosurfactant co-occurs with the cannibalism toxin

SKF at the outer zone of the biofilm. For surfactin, the localization can be explained due to its surface tension lowering attributes, which also facilitates the spreading and expansion of multicellular colonies on the substrate (Angelini et al., 2009). For SKF, this co-localization raises the question if this peptide might also act as a surface-active compound involved in biofilm expansion, rather than killing for nutrients. This new perspective on the role of SKF is further supported by preliminary data on the three-dimensional resolution of toxin distribution in thin sections of *B. subtilis* biofilms, where SKF is predominantly found underneath the biofilm, that is, at the interphase to the agar surface (personal communication K. Dreisewerd, (Wüpping, 2024)) (Fig. 6). This finding demonstrates the considerable potential of resolving toxin distribution in three dimensions. Moreover, it highlights the need for continued advancement in the field, notwithstanding the substantial progress in methodology and technology in recent decades (Brockmann et al., 2019; Dreisewerd et al., 2022; Gessel et al., 2014; Zhu et al., 2022). Further development of the methodology for investigating bacterial biofilms will, therefore, significantly enhance our understanding of the localization of the relevant biomolecules.

Nevertheless, state-of-the-art MALDI-MS imaging technology enabled us to analyze the distribution of EPE, SDP and SKF across biofilms of *B. subtilis* and cannibalistic mutants. This allowed gaining a comprehensive picture of the distribution of cannibalism toxins (in 2D), and their changes as a function of genetic manipulations of cannibalism genes. As mentioned before, SKF is concentrated in the center of the biofilm, and minorly found at the outer edges. SDP is present in the inner zone of the biofilm (Fig. 2). A similar pattern of SKF and SDP distribution has previously been reported for *B. subtilis* biofilms grown on MSgg agar by using MALDI-MS imaging (Si et al., 2016). In a third study, the differences in SDP/SKF localization can be attributed to the difference in strains and culture conditions applied: these authors investigated the domesticated strain *B. subtilis* PY79 grown on ISP2 medium, which lead to relatively unstructured biofilms (Liu et al., 2010). The present study builds upon and complements the knowledge generated by these previous studies by adding the EPE toxin to the picture and demonstrating the co-occurrence and interdependence with the other two toxins. The epipeptide EPE is found predominantly within the outer, actively growing zone of the biofilm (Fig. 2). It is known to trigger the CESR and cause cell death via massive membrane perturbations (Benjdia et al., 2017; Popp et al., 2020, 2021).

Our study demonstrates the importance of cannibalism for the structural organization of *Bacillus* biofilms. As we have shown, toxin production is tightly linked to wrinkle formation and colony expansion. While the absence of one toxin can apparently be compensated by the presence of the other two toxins, so that neither *epeX, sdpC*, nor *skfA* mutants display strong phenotypes, the absence of all three toxins at the same time dramatically influences the structure and shape of the biofilm (Fig. 1). Based on our findings and the aspects discussed above, we propose a modified model of cannibalism in *B. subtilis* multicellular life (Fig. 6).

Cannibalism acts as a differentiation strategy that delays the commitment to sporulate. The absence of cannibalism toxins results in hyper-sporulating non-expanding colonies that are

dominated by spores with few vegetative cells. Endospore formation involves mother cell lysis, increasing dead cell abundance in a hypo-cannibalistic environment. The accumulation of dead cells induces mechanical buckling, promoting vertical biofilm growth (Aguilar et al., 2018), which in turn drives sporulation further as cells are pushed away from nutrient sources. In the presence of EPE, SDP, and SKF, hyper-sporulation is prevented by a fine-tuned system of localized PCD, allowing susceptible sibling cells to be sacrificed progressively and simultaneously across the biofilm, thereby structuring the colony so that the nutrients that are provided allow the population to thrive further, thereby also reaching new sources of nutrient at the periphery of the expanding colony. This process ensures lateral colony expansion while suppressing vertical buckling, thereby also restricting sporulation. Together, this allows *B. subtilis* to grow and thrive in competitive environments, such as its natural habitat, the soil.

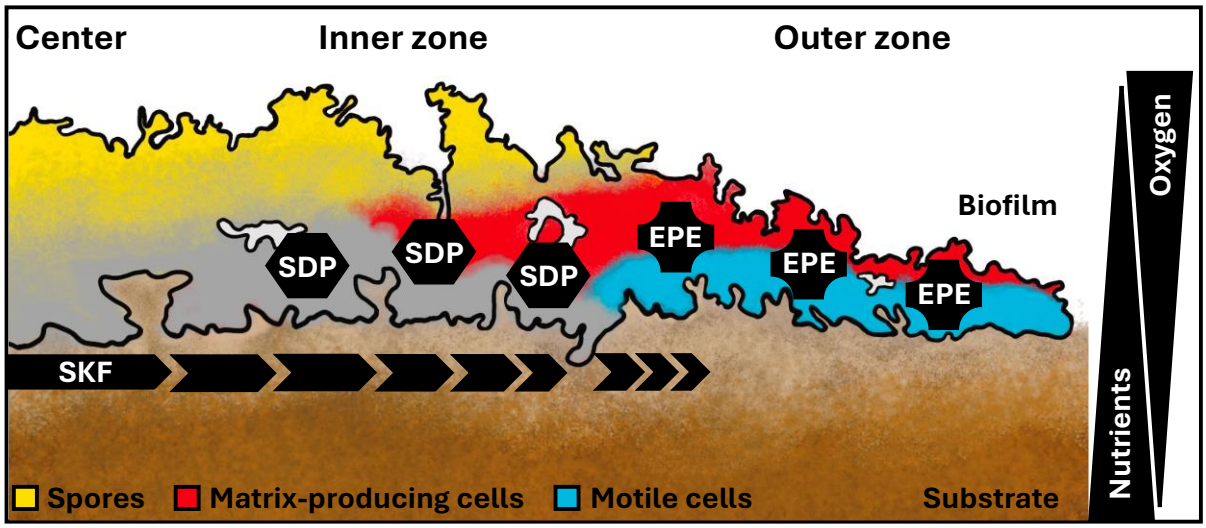

Fig. 6 **Schematic illustration of a *B. subtilis* biofilm cross section showing the distribution of differentiated cell types and cannibalistic toxins SKF, SDP, and EPE across the biofilm.** Based on (Vlamakis et al., 2008).

Production of the ECM is linked to nutrient availability, mainly on the propagating front of the biofilm, but also close to the substrate in older parts of the colony (Srinivasan et al., 2018). These findings are corroborated by our own data concerning the localization of cannibalism toxins: EPE is found at the periphery of the developing biofilm, thereby potentially controlling colony expansion. SKF seems to located at the interface between the biofilm and the substrate (personal communication, K. Dreisewerd, (Wüpping, 2024)), and help colony expansion, in conjunction with surfactin.

Our findings suggest that cannibalism is not merely a survival strategy to delay sporulation, but also a key mechanism to control biofilm development and colony expansion in *B. subtilis*. The interplay between toxin production and differentiation ensures a dynamic and organized colony structure. Future research needs to address the spatiotemporal correlation between swarming, matrix production and sporulation as a function of cannibalism toxin production. While our study sheds important light on the structural role of cannibalism and its functional consequences this has on the phenotypic and cell type distribution within colony biofilms, it also stresses the

importance of bacterial PCD for multicellular differentiation and the structuring of bacterial tissue – a connection that is already well-established for higher eukaryotic tissue but has only emerged recently for bacteria, owing to recent technological breakthroughs that finally allow resolving bacterial macroscopic structures at or at least near single cell resolution (Espinoza Miranda et al., 2025). It seems that the time is ripe to study bacterial tissue formation.

Materials and Methods

Reagents

Chemicals used in this study were obtained from *Thermo Scientific* (Waltham, MA, USA), *Carl Roth GmbH & Co. KG* (Karlsruhe, Germany) or *Sigma-Adrich* (St. Louis, MO, USA). All enzymes (restriction endonucleases, ligases and polymerases for PCR) originated from *New England Biolabs* (Ipswich, MA, USA) and general cloning procedures were performed according to the recommended protocols. PCR purifications and plasmid preparations were undertaken using the corresponding kits from *Süd-Laborbedarf GmbH* (Gauting, Germany).

DNA Isolation

Isolation of genomic DNA from *B. subtilis* for transformation. 800 µl of overnight culture was transferred into a 2 ml Eppendorf tube and mixed with an equal volume of SC buffer (NaCl 0.15 M, sodium citrate 0.01 M, pH 7.0). Cells were then harvested by centrifugation at 13,300 rpm for 1 min and afterwards resuspended in 1 ml SC buffer. 20 µl lysozyme (15 mg/ml) was added and the mix was incubated at 37 °C for 15 min. Afterwards, 800 µl of 5 M NaCl and 200 µl H_2O were added, followed by filtration of the DNA solution through a 0,45 µm syringe filter (*Sarstedt AG & Co. KG*, Nümbrecht, Germany). The DNA solution was directly used for the transformation of *B.subtilis*, or, otherwise stored for later use at -20 °C.

Isolation of total DNA from *B. subtilis*. For isolation and rapid purification of highly pure genomic DNA of *B.subtilis*, the NucleoSpin Microbial DNA (*Macherey-Nagel GmbH & Co. KG,* Düren, Germany) kit was used, following the manufacturer's instructions.

Strain Construction

All oligonucleotides and strains used in this study are listed Table 1 and Table 2, respectively. The synthesis of oligonucleotides was performed by *Microsynth AG* (Balgach, Switzerland). DNA sequencing was performed by *Eurofins Genomics Europe Shared Services GmbH* (Ebersberg, Germany).

The *epeXEPAB* deletions in *B. subtilis* were constructed by allelic replacement mutagenesis using long flanking homology – PCR (LFH-PCR). The technique is derived from a published procedure (Wach, 1996) and was performed as described previously (Jordan et al., 2006; Mascher et al., 2003). The kanamycin resistance cassette was amplified from the suitable template vector pDG780 (Guérout-Fleury et al., 1995), using TM0137/TM0138. Two primer pairs were designed to amplify ~1,000 bp DNA fragments flanking the region to be deleted at its 5' and 3' ends (TM7999/TM8000, and TM8001/TM8002). The resulting fragments are here called the "up" and "do" fragments. The 3' end of the up fragment as well as the 5' end of the do fragment extended into the gene(s) to be deleted in a way that all expression signals of genes up- and downstream of the targeted genes remained intact. Extensions of ~25 nucleotides were added to the 5' end

of the up-reverse and the do-forward primers that were complementary (opposite strand and inverted sequence) to the 5′ and 3′ ends of the amplified resistance cassette. All obtained fragments were purified using the PCR purification kit from *Süd-Laborbedarf GmbH* (Gauting, Germany). 100 to 150 ng of the up and do fragments and 250 to 300 ng of the resistance cassette were used together with the specific up-forward and do-reverse primers at standard concentrations in a second PCR. In this reaction the three fragments were joined by the 25-nucleotide overlapping complementary ends and simultaneously amplified by normal primer annealing. The PCR products were directly used to transform *B. subtilis*. Transformants were screened by colony PCR, using the up-forward primer with a reverse check primer annealing inside the resistance cassette (TM7999/TM0147). The integrity of the regions flanking the integrated resistance cassette and the cassette itself were verified by sequencing PCR products amplified from chromosomal DNA of the resulting mutants.

All other 3A38 mutants were constructed through re-transformation of the corresponding *B. subtilis* 168 mutants. All source strains were checked by sequencing, as just described above. Transformation of *B. subtilis* was performed as described previously (Sambrook & Russell, 2001), adding 100 µl of chromosomal donor-DNA into the mix. Transformants were screened by colony PCR (oligonucleotides, see Table 1).

Table 1 Oligonucleotides used in this study

Name	**Sequence 5’ -3’**	**Source/ Reference**
TM2262	GAGCGTAGCGAAAAATCC	pBS3Cluxcheckfwd
TM2263	GAAATGATGCTCCAGTAACC	pBS3Cluxcheckrev
TM2505	CTGATTGGCATGGCGATTGC	pBS3Clux sacA front check fwd
TM2506	ACAGCTCCAGATCCTCTACG	pBS3Clux sacA front check rev
TM2507	GTCGCTACCATTACCAGTTG	pBS3Clux sacA back check fwd
TM2508	TCCAAACATTCCGGTGTTATC	pBS3Clux sacA back check rev
TM0148	GTTTTGGTCGTAGAGCACACGG	mls-check rev
TM0149	CGTATGTATTCAAATATATCCTCCTCAC	spec-check rev
TM0147	CTGCCTCCTCATCCTCTTCATCC	kan-check rev
TM0137	CAGCGAACCATTTGAGGTGATAGG	kan-fwd
TM0138	CGATACAAATTCCTCGTAGGCGCTCGG	kan-rev
TM2744	TGGTGCGTTAGGGGTTATGATTGC	skf up fwd
TM3316	GCTTCCCTAAGCTGTATTTGAACC	skfA do rev
TM2747	GATTTGCTGCCGTTTTGGTAAGAC	skf do rev
TM3657	CAGCAAGCATAATTTCAAATATCAG	sdpRI do rev LFH

TM7699	TGGCACATACTATTCGCAAAA	sdpR_BKE_checkfwd
TM2748	GAAGGTTATATTGACACCTATAATCC	sdpC up fwd
TM2751	CAAATATCTAAATGTCTAAATGTTTTTTTGTAAAG	sdpC do rev
TM5426	GTGATCAGCTTATCGGCTTG	yydF(epeX)-up-fwd
TM8140	GGATAGAAGTAGTTTATTTTTTCTGC	oLF_epeX_rev
TM5430	GAGGAATTTGACATTCCTTATG	yydI-up-fwd
TM8143	CTAGCCATCTTTGCGCTC	oLF_epeA_rev
TM3324	CATCGTTTTAGTAATGATCTGACC	skfEF do rev
TM3321	CAGTACTTATTGGTACATAGCGG	skfEF up fwd
TM7766	ATGTCAGCAAACATCGCAC	oLF_sdpABCRI up_fwd
TM7769	ACTGTTCACCGGTGATTCC	oLF_sdpABCRI do_rev
TM3655	GATGAATTGAAACAATCGATTGACAG	sdpR do rev LFH
TM7999	CGGTGATCAGCTTATCG	oLF_EPE_upfwd
TM8000	CCTATCACCTCAAATGGTTCGCTGATCCCTCCTCC TTTTC	oLF_EPE_uprev
TM8001	CGAGCGCCTACGAGGAATTTGTATCGGCCTTTAAT AAAGGGAGCTAC	oLF_EPE_dofwd
TM8002	TACCAGCAAATCGCAAC	oLF_EPE_dorev
TM7503	CCGCTCGGATAATAAATCGG	oNB_PabrB_seq_fwd
TM7504	CGATAGGAATAACTACACGTCC	oNB_PabrB_seq_rev

Table 2 Strains used and generated in this study.

Name	**Genotype and Relevant Features**	**Source / Reference**
3A38 (WT)	*comI*^{Q12L} , undomesticated competent wild type strain	(Konkol et al., 2013)
TMB7067	*B. subtilis 3A38 epeX::mls*	This study
TMB6126	*B. subtilis 3A38 epeAB::spec*	This study
TMB6336	*B. subtilis 3A38 epeAB::spec* “flare” mutation	This study
TMB6363	*B. subtilis 3A38 epeAB::spec* “flare” mutation	This study
TMB6364	*B. subtilis 3A38 epeAB::spec* “flare” mutation	This study
TMB6365	*B. subtilis 3A38 epeAB::spec* “flare” mutation	This study
TMB6366	*B. subtilis 3A38 epeAB::spec* “flare” mutation	This study
TMB7060	*B. subtilis 3A38 sdpC::kan*	This study
TMB7056	*B. subtilis 3A38 sdpI::mls*	This study
TMB7069	*B. subtilis 3A38 skfA::mls*	This study
TMB6978	*B. subtilis 3A38 skfEF::mls*	This study
TMB6980	*B. subtilis 3A38 epeXEPAB::kan, skfABCEFGH::spec, sdpABCRI::tet*	This study
TMB6136	*B. subtilis 3A38 sacA::*pBS3C*lux*-P$_{lial}$	This study
TMB6170	*B. subtilis 3A38 sacA::*pBS3C*lux*-P$_{epeX}$	This study
TMB6171	*B. subtilis 3A38 sacA::cat* pBS3C*lux*-P$_{empty}$	This study

TMB6217	*B. subtilis 3A38 sacA*::pBS3C*lux*-P_{liaI}, *epeAB*::*spec*	This study
TMB6220	*B. subtilis 3A38 sacA*::pBS3C*lux*-$P_{liaI,}$ *epeX*::*ery*	This study
TMB6351	*B. subtilis 3A38 sacA*::pBS3C*lux*-P_{sdpA}	This study
TMB7278	*B. subtilis 3A38 sacA*::pBS3C*lux*-P_{sdpA}, *sdpI*::*mls*	This study
TMB6733	*B. subtilis 3A38 sacA*::pBS3C*lux*-P_{skfA}	This study
TMB7277	*B. subtilis 3A38 sacA*::pBS3C*lux*-P_{skfA}, *skfEF::mls*	This study
TMB7279	*B. subtilis 3A38 sacA*::pBS3C*lux*-P_{bceA}	This study
TMB7280	*B. subtilis 3A38 sacA*::pBS3C*lux*-P_{bceA}, *sdpI*::*mls*	This study
TMB7281	*B. subtilis 3A38 sacA*::pBS3C*lux*-P_{bceA}, *skfEF::mls*	This study
TMB7282	*B. subtilis 3A38 sacA*::pBS3C*lux*-P_{psdA}	This study
TMB7283	*B. subtilis 3A38 sacA*::pBS3C*lux*-P_{psdA}, *sdpI*::*mls*	This study
TMB7284	*B. subtilis 3A38 sacA*::pBS3C*lux*-P_{psdA}, *skfEF::mls*	This study
BKE40180	*B.* subtilis 168 yydF(epeX)::erm	(Koo et al., 2017)
HB6267	*B. subtilis CU1065 yydIJ(epeAB)::spec*	(Butcher et al., 2007)
TMB1768	*B. subtilis 168 sdpC::kan*	(Höfler et al., 2016)
BKE33780	*B. subtilis 168 sdpI::erm*	(Koo et al., 2017)
BKE01910	*B. subtilis 168 skfA::erm*	(Koo et al., 2017)
TMB2262	*B. subtilis 168 skfEF::erm*	(Höfler et al., 2016)
TMB6911	*B. subtilis 3A38 epeXEPAB::kan skfA-H::spec*	This study
TMB6896	*B. subtilis 3A38 epeXEPAB::kan*	This study
TMB1771	*B. subtilis 168 skfABCEFGH::spec*	This study
EG494	*B. subtilis PY79 sdpABCIR::tet*	(Ellermeier et al., 2006)
TMB3822	*B. subtilis 168 sacA*::P_{liaI}-*luxABCDE*	(Popp et al., 2017)
TMB4178	*B. subtilis 168 pBS3Clux-PepeX*	(Popp et al., 2021)
TMB2841	*B. subtilis 168 sacA*::*luxABCDE (empty vector)*	(Pinto et al., 2018)
Nr. 8	*E. coli* pDG780 (source of kan cassette for LFH-PCR)	(Guérout-Fleury et al., 1995)

Growth Conditions

The bacterial strains used in the present study are listed in Table 2. For routine growth of *Bacillus subtilis*, lysogeny broth liquid media was made using the following recipe: 1% (w/v) Bacto-peptone, 1% (w/v) NaCl, 0.5% (w/v) yeast extract. For solid plates, LB broth was supplemented with 1.5% (w/v) agar. LB media was sterilized by autoclaving. For transformation of *B. subtilis*, chemically defined medium MNGE [88.2% 1 × MN medium (1.36% (w/v) dipotassium phosphate × 3 H_2O, 0.6% (w/v) monopotassium phosphate, 0.1% (w/v) sodium citrate × H_2O), 1.9% glucose, 0.19% potassium glutamate, 0.001% (w/v) ammonium ferric citrate, 0.005% (w/v) tryptophan, and 0.035% (w/v) magnesium sulfate] was used. Single isolate biofilm assays were conducted using MSgg (Minimal Salts glycerol glutamate) medium. MSgg was made by first preparing a base medium, consisting of 5 mM potassium phosphate, 100 mM MOPS at pH 7.0, supplemented with 1.5% (w/v) agar. The base medium was autoclaved and cooled to 55 °C. The base medium was supplemented with 2 mM $MgCl_2$, 700 µM $CaCl_2$, 50 µM $FeCl_3$, 50 µM $MnCl_2$, 1 µM $ZnCl_2$, 2 µM thiamine, 0.5% (v/v) glycerol and 0.5% (w/v) glutamic acid. A volume of 25 ml of MSgg melted medium was added to each 10 cm square petri dish (*Sarstedt AG & Co. KG*, Nümbrecht, Germany) and solidified at room temperature. The surface of the solid plates was dried for 45 min under a laminar flow cabinet before use in experiments.

B. subtilis cells carrying a resistance marker were selected using spectinomycin (100 µg/ml), tetracycline (12.5 µg/ml), kanamycin (10 µg/ml), or erythromycin (1 µg/ml) combined with lincomycin (25 µg/ml) for MLS.

Biofilm formation assay

For growing biofilms, overnight cultures in LB medium with selective antibiotics were diluted to OD_{600} 0.1 in 1 ml LB medium. Carefully, 5 µl of the cell suspension were spotted on MSgg agar plates, which were dried for 45 min beforehand as previously described. For MALDI-MS-Imaging (MALDI-MS-I) analysis and flow cytometry, 5 µl of the cell suspension were spotted onto a 0.22 µm pore size mixed-cellulose-esters filter membrane (*Merck Millipore*, Darmstadt, Germany) which was placed on MSgg agar. Agar plates were incubated at 25 °C. Pictures were taken daily using a P.CAM360 (*TU Dresden*, Dresden, Germany) or a binocular microscope WILD M3Z (*Leica Microsystems GmbH*, Wetzlar, Germany) with a ProgRes “SpeedXT core5” camera (*Jenoptik AG*, Jena, Germany; Capture Pro software) over the course of 8 days. Assays were performed in biological duplicates and technical triplicates.

Luciferase Assay

For luciferase assays on MSgg agar plates, biofilms were grown as previously described. Luminescence was detected with a Fusion FX system (*Vilber Lourmat GmbH*, Eberhardzell, Germany). The exposure times for the luminescence reporters were as followed: P_{epeX} 5 s; P_{sdpA}

and P_{skfA} 10 s; P_{bceA}, P_{psdA}, P_{liaI} and P_{empty} 2 min. Assays were performed in biological duplicates and technical triplicates.

MALDI-MS Imaging

Biofilms were grown on mixed cellulose ester membranes with 0.22 µm average pore size following the procedure described earlier. The membranes were used to ensure easy detachment of the biofilms from the agar and to simplify subsequent inactivation as described by Brockmann and colleagues (Brockmann et al., 2019). For fixation and microscopy, bacterial biofilms were cut out and wetted with a solution of 10% (v/v) formaldehyde (*Carl Roth GmbH & Co. KG*, Karlsruhe, Germany) in water. After 30 min, fixation was complete and the biofilms were washed two times with Milli-Q water (*Merck KGaA*, Darmstadt, Germany) and then glued together with the membrane on a microscope slide using super glue (*UHU GmbH & Co KG*, Bühl, Germany). A VS200 slide scanner with a 4x objective (*Evident GmbH*, Hamburg, Germany) and ORCA-Fusion C14440 20UP camera (*Hamamatsu photonics*, Hamamatsu City, Japan) was used for reflected light microscopy of biofilms. For microscope image visualization, OlyVia (version 3.4.1, *Evident,* Hamburg, Germany) was used. A solution of 7 mg/ml 2,5-dihydroxyacetophenone (*Merck KgaA*, Darmstadt, Germany) solved in 75% acetonitrile (*Carl Roth GmbH & Co. KG*, Karlsruhe, Germany), 10% methanol (*Carl Roth GmbH & Co. KG*, Karlsruhe, Germany), 10% trifluoroacetic acid (*Carl Roth GmbH & Co. KG*, Karlsruhe, Germany) and 5% Milli-Q water was sprayed on the biofilm as MALDI matrix using a SunCollect pneumatic spray roboter (*SunChrom*, Friedrichsdorf, Germany). The matrix was applied within 22 spraying cycles at a nitrogen back pressure of 2.5 bar in a meandering pattern. The flow rate followed a gradient and started at 15 µl/min in the first cycle and increased to 20 µl/min and 30 µl/min for the second and third spraying cycle, respectively. From the fourth spraying cycle onwards, the flow rate was 50 µl/min until the end. The spray nozzle moved with a velocity of 700 mm/min and a line distance of 2 mm. The distance between the spray nozzle and sample surface was set to 44 mm.

All MALDI-MSI measurements were conducted with a Bruker timsTOF fleX MALDI-2 QTOF mass spectrometer (*Bruker Daltonics*, Bremen, Germany), equipped with a Smartbeam3DTM laser emitting at 355 nm providing a focal spot size of 5 µm diameter. For all imaging experiments, the resulting field size was 50 µm using beam scan function and the “M5 small” setting with 200 laser shots per pixel with a frequency of 1 kHz and a nitrogen pressure in the MALDI source of 2.5 mbar. With the analytical focus on the detection of the peptide toxins, all herein reported MSI data were acquired in the “High sensitivity Detection” mode within a m/z range of 1000 – 4500 in positive ion mode and with the MALDI-2-postionization disabled. MSI data was processed using SCiLS Lab MVS (vs. 2024a Pro, *Bruker Daltonics*, Bremen, Germany) and ion images visualized as false color imaging using the same software. MSI experiments were performed in biological and technical duplicates.

Microbial flow cytometry and cytometric fingerprinting

Flow cytometric analysis followed the procedure described by (Abbaszade et al., 2025). In short: a BD Influx v7 Cell Sorter, (Becton Dickinson, Franklin Lakes, NJ, USA) equipped with a stream-in-air nozzle of 70 µm was used. The blue 488 nm Sapphire OPS laser (400 mW) was used for measurement of the forward scatter (FSC, 488/10; PMT1; related to cell size), the side scatter (SSC, trigger signal, 488/10; PMT2; related to cell density), the SYTO9 fluorescence (530/40; PMT3), and the PI fluorescence (616/23; PMT5). The UV laser 355 nm Genesis OPS laser (100 mW) was used to measure DAPI fluorescence (460/50; PMT9). The fluidics ran at 33 psi through a 70 µm nozzle and cells were detected equivalent to an event rate of 2,500 to 3,000 events sec^{-1}. The calibration of the cytometer was performed in the linear range by using 1 µm blue fluorescent FluoSpheres (Ref. F-8815, Molecular Probes, Eugene, OR, USA), 2 µm YG fluorescent FluoSpheres (Ref. F-8827, ThermoFisher Scientific, Waltham, MA, USA). For calibration in the logarithmic range, 0.5 µm and 1 µm YG fluorescent FluoSpheres (Ref. F-8813 and F-13081, ThermoFisher Scientific, Waltham, MA, USA) were used. The obtained flow cytometry data were stored in the Zenodo database under the following DOI: https://zenodo.org/records/14967544. Biopsy samples were taken from one biological replicate using a 200 µl pipette tip from six different positions, covering the biofilm from the center to the outer edge. Based on a low cell count, biopsy samples were not OD-adjusted during cell handling. For analysis of population heterogeneity related to cell cycle states, DAPI staining was performed as described in (Abbaszade et al., 2025). For discrimination between live and compromised cells, the combination of SYTO9 and PI staining was used as described in (Abbaszade et al., 2025). For each bacterial strain, 50.000 cells were measured flow cytometrically and visualized in 2D plots using the program FlowJo 10.0.8.r1 (FlowJo, Becton Dickinson, Franklin Lakes, NJ, USA). Cell gate setting and the creation of the gate template was done as suggested by (Abbaszade et al., 2025). FACSorting of different cell types for fluorescence microscopy were done using the gates from the gate template. For each gate, 50.000-200.000 cells were sorted. Data analysis followed the description published elsewhere (Abbaszade et al., 2025).

Fluorescence Microscopy

Agarose pads were used as a measure to immobilize the spores in preparation for microscopy. Therefore, 1% UltraPure Agarose (*Life Technologies GmbH*, Darmstadt, Germany) was added to a rubber mold sticking to a slide and covered with a second slide until hardened. Size measurements were 20 mm in diameter and about 1 mm in depth. 2 µl of cell suspension was added on top of the agarose pads and covered with a coverslip. The prepared slides were analyzed using the Zeiss AXIO Observer Z1 (*Carl Zeiss AG*, Oberkochen, Germany) with an Axiocam 503 mono *Carl Zeiss AG*, Oberkochen, Germany) at a total magnitude of 630x (immersion objective PlanApo 63x/ 1.40 Oil Ph3 M27, NA1.4). Microscopy was performed using phase-contrast (Ph3, light intensity: 4.4 V, exposure time: 1.59 s) and BFP-channel (exposure

time: 3.13 s for gates: c1n, c2n, c3n, csp1, sp1; 1.81 s for gates sp3, sp4). Excitation wavelength and emission wavelength were 353 nm and 465 nm, respectively. Analysis of the microscopy images was performed using the software Fiji ("ImageJ"). Rectangles were cropped from the original image representative for cells of each cell type.

Whole Genome Sequencing and Comparison

Genomic DNA was isolated with the NucleoSpin® Microbial DNA Kit according to the manufacturer's protocol. Whole genome sequencing was performed by the Microbial Functional Genomics Group (LMU, Munich, Germany) using Sanger/Illumina 1.9 (paired end read) for analysis of the *epeAB* mutant flare (TMB6336).

Data analysis was performed using the open-source platform Galaxy EU (24.1) (*usegalaxy.eu*, Freiburg Galaxy Team). For TMB6336, quality of the Illumina paired-end data was verified with "FastQC" (Galaxy v.0.11.8) (Andrews, n.d.). To automate quality and adapter trimming, the sequencing data were analyzed with "Trim Galore!" (Galaxy v.0.4.3.1; threshold: 20; maximum error rate: 0.1; minimum reads length: 20) and sequences bearing an average quality below the threshold value were subsequently removed using "Trimmomatic" (Galaxy v.0.36.5; Average quality required: 20; Number of bases to average across: 4) (Bolger et al., 2014). High-quality paired-end data were then assembled as contigs using "Unicycler" (Galaxy v.0.4.8.0; minimum length of contigs: 100 bp) (Wick et al., 2017). Quality check of the assembled genome was performed using "Quast" (Gurevich et al., 2013; Mikheenko et al., 2016, 2018). Subsequently, the genome assembly contigs were aligned with the genome of *Bacillus subtilis* (ASM904v1) using the "RagTag" tool (reference-guided scaffolding of draft genomes; Galaxy Version 2.1.0+galaxy1) (Alonge et al., 2019). For genome annotation, the software tool "Prokka" was used (Cuccuru et al., 2014; Seemann, 2014). The assembled genome was aligned to the reference genome to find single nucleotide polymorphisms (SNPs), insertions and deletions using the "snippy" tool with the default parameters (Galaxy Version 3.2) (Seemann, 2015). For visualization, the script "JBrowse genome" (Version 1.16.11) was used (Skinner et al., 2009).

Acknowledgments

This work was supported by the German Research Foundation (DFG) within the priority program SPP 2389 “Emergent Functions of Bacterial Multicellularity” (Grants K.D. and T.M.: 504017689, S.M.: 503905203). We thank Jens Soltwisch for helpful discussions and Kim Wüpping (U. Münster) for offering preliminary results of cross sections and enable a more in-depth discussion of the method, Denis Iliasov and Daniela Hartmann for support during WGS analysis using the Galaxy platform, and Bruker Daltonics (Bremen, Germany) for valuable technical support.

Conflict of interest statement

None declared.

Literature

Abbaszade, G., Stückrath, K., & Müller, S. (2025). Bacterial colony biopsies: spatial discrimination of heterogeneous cell types by cytometric fingerprinting. *Methods in Ecology and Evolution* (accepted). http://biorxiv.org/lookup/doi/10.1101/2024.11.25.623575

Aguilar, B., Ghaffarizadeh, A., Johnson, C. D., Podgorski, G. J., Shmulevich, I., & Flann, N. S. (2018). Cell death as a trigger for morphogenesis. *PLoS ONE*, *13*. https://doi.org/10.1371/journal.pone.0191089

Alonge, M., Soyk, S., Ramakrishnan, S., Wang, X., Goodwin, S., Sedlazeck, F. J., Lippman, Z. B., & Schatz, M. C. (2019). RaGOO: Fast and accurate reference-guided scaffolding of draft genomes. *Genome Biology*, *20*. https://doi.org/10.1186/s13059-019-1829-6

Andrews, S. (n.d.). *FastQC - A Quality Control tool for High Throughput Sequence Data*.

Angelini, T. E., Roper, M., Kolter, R., Weitz, D. A., & Brenner, M. P. (2009). Bacillus subtilis spreads by surfing on waves of surfactant. *Proceedings of the National Academy of Sciences of the United States of America*, *106*, 18109–18113. https://doi.org/10.1073/pnas.0905890106

Arnaouteli, S., Bamford, N. C., Stanley-Wall, N. R., & Kovács, Á. T. (2021). Bacillus subtilis biofilm formation and social interactions. In *Nature Reviews Microbiology* (Vol. 19, pp. 600–614). Nature Research. https://doi.org/10.1038/s41579-021-00540-9

Asally, M., Kittisopikul, M., Rué, P., Du, Y., Hu, Z., Çağatay, T., Robinson, A. B., Lu, H., Garcia-Ojalvo, J., & Süel, G. M. (2012). Localized cell death focuses mechanical forces during 3D patterning in a biofilm. *Proceedings of the National Academy of Sciences of the United States of America*, *109*(46), 18891–18896. https://doi.org/10.1073/pnas.1212429109

Azulay, D. N., Spaeker, O., Ghrayeb, M., Wilsch-Bräuninger, M., Scoppola, E., Burghammer, M., Zizak, I., Bertinetti, L., Politi, Y., & Chai, L. (2022). Multiscale X-ray study of Bacillus subtilis biofilms reveals interlinked structural hierarchy and elemental heterogeneity. *Proceedings of the National Academy of Sciences of the United States of America*, *119*. https://doi.org/10.1073/pnas.2118107119

Benjdia, A., Guillot, A., Ruffié, P., Leprince, J., & Berteau, O. (2017). Post-translational modification of ribosomally synthesized peptides by a radical SAM epimerase in Bacillus subtilis. *Nature Chemistry*, *9*, 698–707. https://doi.org/10.1038/nchem.2714

Besharova, O., Suchanek, V. M., Hartmann, R., Drescher, K., & Sourjik, V. (2016). Diversification of gene expression during formation of static submerged biofilms by Escherichia coli. *Frontiers in Microbiology*, *7*. https://doi.org/10.3389/fmicb.2016.01568

Bolger, A. M., Lohse, M., & Usadel, B. (2014). Trimmomatic: A flexible trimmer for Illumina sequence data. *Bioinformatics*, *30*, 2114–2120. https://doi.org/10.1093/bioinformatics/btu170

Branda, S. S., González-Pastor, J. E., Ben-Yehuda, S., Losick, R., & Kolter, R. (2001). Fruiting body formation by Bacillus subtilis. *Proceedings of the National Academy of Sciences of the United States of America*, *98*, 11621–11626. https://doi.org/10.1073/pnas.191384198

Brockmann, E. U., Steil, D., Bauwens, A., Soltwisch, J., & Dreisewerd, K. (2019). Advanced Methods for MALDI-MS Imaging of the Chemical Communication in Microbial Communities. *Analytical Chemistry*, *91*, 15081–15089. https://doi.org/10.1021/acs.analchem.9b03772

Burbulys, D., Trach, K. A., & Hoch, J. A. (1991). Initiation of sporulation in B. subtilis is controlled by a multicomponent phosphorelay. *Cell*, *64*, 545–552. https://doi.org/10.1016/0092-8674(91)90238-T

Chai, L., Zaburdaev, V., & Kolter, R. (2024). How bacteria actively use passive physics to make biofilms. *Proceedings of the National Academy of Sciences of the United States of America*, *121*, e2403842121. https://doi.org/10.1073/pnas.2403842121

Chai, Y., Chu, F., Kolter, R., & Losick, R. (2008). Bistability and biofilm formation in Bacillus subtilis. *Molecular Microbiology*, *67*, 254–263. https://doi.org/10.1111/j.1365-2958.2007.06040.x

Chu, F., Kearns, D. B., Branda, S. S., Kolter, R., & Losick, R. (2006). Targets of the master regulator of biofilm formation in Bacillus subtilis. *Molecular Microbiology*, *59*, 1216–1228. https://doi.org/10.1111/j.1365-2958.2005.05019.x

Cuccuru, G., Orsini, M., Pinna, A., Sbardellati, A., Soranzo, N., Travaglione, A., Uva, P., Zanetti, G., & Fotia, G. (2014). Orione, a web-based framework for NGS analysis in microbiology. *Bioinformatics*, *30*, 1928–1929. https://doi.org/10.1093/bioinformatics/btu135

Dar, D., Dar, N., Cai, L., & Newman, D. K. (2021). Spatial transcriptomics of planktonic and sessile bacterial populations at single-cell resolution. *Science*, *373*. https://doi.org/10.1126/science.abi4882

De Kievit, T. R., Gillis, R., Marx, S., Brown, C., & Iglewski, B. H. (2001). Quorum-Sensing Genes in Pseudomonas aeruginosa Biofilms: Their Role and Expression Patterns. *Applied and Environmental Microbiology*, *67*, 1865–1873. https://doi.org/10.1128/AEM.67.4.1865-1873.2001

De la Fuente-Núñez, C., Reffuveille, F., Fernández, L., & Hancock, R. E. W. (2013). Bacterial biofilm development as a multicellular adaptation: Antibiotic resistance and new therapeutic strategies. In *Current Opinion in Microbiology* (Vol. 16, pp. 580–589). https://doi.org/10.1016/j.mib.2013.06.013

Dinesen, C., Vertot, M., Jarmusch, S. A., Lozano-Andrade, C. N., Andersen, A. J. C., & Kovács, Á. T. (2025). Subtilosin A production is influenced by surfactin levels in Bacillus subtilis. *MicroLife*, *6*, uqae029. https://doi.org/10.1093/femsml/uqae029

Donovan, W., Zheng, L., Sandman, K., & Losick, R. (1987). Genes encoding spore coat polypeptides from Bacillus subtilis. *Journal of Molecular Biology*, *196*, 1–10. https://doi.org/10.1016/0022-2836(87)90506-7

Dreisewerd, K., Bien, T., & Soltwisch, J. (2022). MALDI-2 and t-MALDI-2 Mass Spectrometry Imaging. In *Methods in Molecular Biology* (Vol. 2437, pp. 21–40). Humana Press Inc. https://doi.org/10.1007/978-1-0716-2030-4_2

Ellermeier, C. D., Hobbs, E. C., Gonzalez-Pastor, J. E., & Losick, R. (2006). A three-protein signaling pathway governing immunity to a bacterial cannibalism toxin. *Cell*, *124*, 549–559. https://doi.org/10.1016/j.cell.2005.11.041

Espinoza Miranda, S. S., Abbaszade, G., Hess, W. R., Drescher, K., Saliba, A.-E., Zaburdaev, V., Chai, L., Dreisewerd, K., Grünberger, A., Westendorf, C., Müller, S., & Mascher, T. (2025). Resolving spatiotemporal dynamics in bacterial multicellular populations: approaches and challenges. *Microbiology and Molecular Biology Reviews*. https://doi.org/10.1128/mmbr.00138-24

Flemming, H. C., Baveye, P., Neu, T. R., Stoodley, P., Szewzyk, U., Wingender, J., & Wuertz, S. (2021). Who put the film in biofilm? The migration of a term from wastewater engineering to medicine and beyond. In *npj Biofilms and Microbiomes* (Vol. 7). Nature Research. https://doi.org/10.1038/s41522-020-00183-3

Fujita, M., González-Pastor, J. E., & Losick, R. (2005). High- and low-threshold genes in the Spo0A regulon of Bacillus subtilis. *Journal of Bacteriology*, *187*, 1357–1368. https://doi.org/10.1128/JB.187.4.1357-1368.2005

Gessel, M. M., Norris, J. L., & Caprioli, R. M. (2014). MALDI imaging mass spectrometry: Spatial molecular analysis to enable a new age of discovery. In *Journal of Proteomics* (Vol. 107, pp. 71–82). Elsevier. https://doi.org/10.1016/j.jprot.2014.03.021

González-Pastor, J. E. (2011). Cannibalism: A social behavior in sporulating Bacillus subtilis. In *FEMS Microbiology Reviews* (Vol. 35, pp. 415–424). https://doi.org/10.1111/j.1574-6976.2010.00253.x

González-Pastor, J. E., Hobbs, E. C., & Losick, R. (2003). Cannibalism by sporulating bacteria. *Science*, *301*, 510–513. https://doi.org/10.1126/science.1086462

Guérout-Fleury, A. M., Shazand, K., Frandsen, N., & Stragier, P. (1995). Antibiotic-resistance cassettes for Bacillus subtilis. *Gene*, *167*, 335–336. https://doi.org/10.1016/0378-1119(95)00652-4

Gurevich, A., Saveliev, V., Vyahhi, N., & Tesler, G. (2013). QUAST: Quality assessment tool for genome assemblies. *Bioinformatics*, *29*, 1072–1075. https://doi.org/10.1093/bioinformatics/btt086

Hamon, M. A., & Lazazzera, B. A. (2001). The sporulation transcription factor Spo0A is required for biofilm development in Bacillus subtilis. *Molecular Microbiology*, *42*, 1199–1209. https://doi.org/10.1046/j.1365-2958.2001.02709.x

Höfler, C., Heckmann, J., Fritsch, A., Popp, P., Gebhard, S., Fritz, G., & Mascher, T. (2016). Cannibalism stress response in Bacillus subtilis. *Microbiology (United Kingdom)*, *162*(1), 164–176. https://doi.org/10.1099/mic.0.000176

Hullo, M. F., Moszer, I., Danchin, A., & Martin-Verstraete, I. (2001). CotA of Bacillus subtilis is a copper-dependent laccase. *Journal of Bacteriology*, *183*, 5426–5430. https://doi.org/10.1128/JB.183.18.5426-5430.2001

Jordan, S., Hutchings, M. I., & Mascher, T. (2008). Cell envelope stress response in Gram-positive bacteria. In *FEMS Microbiology Reviews* (Vol. 32, pp. 107–146). https://doi.org/10.1111/j.1574-6976.2007.00091.x

Jordan, S., Junker, A., Helmann, J. D., & Mascher, T. (2006). Regulation of LiaRS-Dependent Gene Expression in Bacillus subtilis: Identification of Inhibitor Proteins, Regulator Binding Sites, and Target Genes of a Conserved Cell Envelope Stress-Sensing Two-Component System. *Journal of Bacteriology*, *188*(14). https://doi.org/10.1128/JB.00310-06

Koo, B. M., Kritikos, G., Farelli, J. D., Todor, H., Tong, K., Kimsey, H., Wapinski, I., Galardini, M., Cabal, A., Peters, J. M., Hachmann, A. B., Rudner, D. Z., Allen, K. N., Typas, A., & Gross, C. A. (2017). Construction and Analysis of Two Genome-Scale Deletion Libraries for Bacillus subtilis. *Cell Systems*, *4*, 291-305.e7. https://doi.org/10.1016/j.cels.2016.12.013

Lamsa, A., Liu, W. T., Dorrestein, P. C., & Pogliano, K. (2012). The Bacillus subtilis cannibalism toxin SDP collapses the proton motive force and induces autolysis. *Molecular Microbiology*, *84*, 486–500. https://doi.org/10.1111/j.1365-2958.2012.08038.x

Liu, W. T., Yang, Y. L., Xu, Y., Lamsa, A., Haste, N. M., Yang, J. Y., Ng, J., Gonzalez, D., Ellermeier, C. D., Straight, P. D., Pevzner, P. A., Pogliano, J., Nizet, V., Pogliano, K., & Dorrestein, P. C. (2010). Imaging mass spectrometry of intraspecies metabolic exchange revealed the cannibalistic factors of Bacillus subtilis. *Proceedings of the National Academy of Sciences of the United States of America*, *107*, 16286–16290. https://doi.org/10.1073/pnas.1008368107

Lopez, D., Vlamakis, H., & Kolter, R. (2009). Generation of multiple cell types in Bacillus subtilis. In *FEMS Microbiology Reviews* (Vol. 33, pp. 152–163). https://doi.org/10.1111/j.1574-6976.2008.00148.x

López, D., Vlamakis, H., Losick, R., & Kolter, R. (2009). Cannibalism enhances biofilm development in bacillus subtilis. *Molecular Microbiology*, *74*, 609–618. https://doi.org/10.1111/j.1365-2958.2009.06882.x

Mascher, T., Margulis, N. G., Wang, T., Ye, R. W., & Helmann, J. D. (2003). Cell wall stress responses in Bacillus subtilis: the regulatory network of the bacitracin stimulon. *Molecular Microbiology*, *50*(5). https://doi.org/10.1046/j.1365-2958.2003.03786.x

Mikheenko, A., Prjibelski, A., Saveliev, V., Antipov, D., & Gurevich, A. (2018). Versatile genome assembly evaluation with QUAST-LG. *Bioinformatics*, *34*, i142–i150. https://doi.org/10.1093/bioinformatics/bty266

Mikheenko, A., Valin, G., Prjibelski, A., Saveliev, V., & Gurevich, A. (2016). Icarus: Visualizer for de novo assembly evaluation. *Bioinformatics*, *32*, 3321–3323. https://doi.org/10.1093/bioinformatics/btw379

Milton, M. E., & Cavanagh, J. (2023). The Biofilm Regulatory Network from Bacillus subtilis: A Structure-Function Analysis. In *Journal of Molecular Biology* (Vol. 435). Academic Press. https://doi.org/10.1016/j.jmb.2022.167923

Molle, V., Fujita, M., Jensen, S. T., Eichenberger, P., González-Pastor, J. E., Liu, J. S., & Losick, R. (2003). The Spo0A regulon of Bacillus subtilis. *Molecular Microbiology*, *50*, 1683–1701. https://doi.org/10.1046/j.1365-2958.2003.03818.x

Newman, J. A., Rodrigues, C., & Lewis, R. J. (2013). Molecular basis of the activity of SinR Protein, the master regulator of biofilm formation in bacillus subtilis. *Journal of Biological Chemistry*, *288*, 10766–10778. https://doi.org/10.1074/jbc.M113.455592

Parsek, M. R., & Tolker-Nielsen, T. (2008). Pattern formation in Pseudomonas aeruginosa biofilms. In *Current Opinion in Microbiology* (Vol. 11, pp. 560–566). https://doi.org/10.1016/j.mib.2008.09.015

Piggot, P. J., & Hilbert, D. W. (2004). Sporulation of Bacillus subtilis. In *Current Opinion in Microbiology* (Vol. 7, pp. 579–586). https://doi.org/10.1016/j.mib.2004.10.001

Pinto, D., Vecchione, S., Wu, H., Mauri, M., Mascher, T., & Fritz, G. (2018). Engineering orthogonal synthetic timer circuits based on extracytoplasmic function factors. *Nucleic Acids Research*, *46*, 7450–7464. https://doi.org/10.1093/nar/gky614

Popp, P. F., Benjdia, A., Strahl, H., Berteau, O., & Mascher, T. (2020). The Epipeptide YydF Intrinsically Triggers the Cell Envelope Stress Response of Bacillus subtilis and Causes Severe Membrane Perturbations. *Frontiers in Microbiology*, *11*. https://doi.org/10.3389/fmicb.2020.00151

Popp, P. F., Friebel, L., Benjdia, A., Guillot, A., Berteau, O., & Mascher, T. (2021). The Epipeptide Biosynthesis Locus epeXEPAB Is Widely Distributed in Firmicutes and Triggers Intrinsic Cell Envelope Stress. *Microbial Physiology*, *31*(3), 306–318. https://doi.org/10.1159/000516750

Popp, P. F., & Mascher, T. (2019). Coordinated Cell Death in Isogenic Bacterial Populations: Sacrificing Some for the Benefit of Many? In *Journal of Molecular Biology* (Vol. 431, pp. 4656–4669). Academic Press. https://doi.org/10.1016/j.jmb.2019.04.024

Qin, Y., Angelini, L. L., & Chai, Y. (2022). Bacillus subtilis Cell Differentiation, Biofilm Formation and Environmental Prevalence. *Microorganisms*, *10*. https://doi.org/10.3390/microorganisms10061108

Radeck, J., Fritz, G., & Mascher, T. (2017). The cell envelope stress response of Bacillus subtilis: from static signaling devices to dynamic regulatory network. In *Current Genetics* (Vol. 63, Issue 1, pp. 79–90). Springer Verlag. https://doi.org/10.1007/s00294-016-0624-0

Rahman, F. Bin, Sarkar, B., Moni, R., & Rahman, M. S. (2021). Molecular genetics of surfactin and its effects on different sub-populations of Bacillus subtilis. In *Biotechnology Reports* (Vol. 32). Elsevier B.V. https://doi.org/10.1016/j.btre.2021.e00686

Sambrook, J., & Russell, D. W. (2001). *Molecular Cloning - a laboratory manual.* (Third Edition, Vol. 3). Cold Spring Harbor Laboratory Press.

Schultz, D., Wolynes, P. G., Jacob, E. Ben, & Onuchic, J. N. (2009). Deciding fate in adverse times: Sporulation and competence in Bacillus subtilis. *Proceedings of the National Academy of Sciences of the United States of America*, *106*, 21027–21034. https://doi.org/10.1073/pnas.0912185106

Seemann, T. (2014). Prokka: Rapid prokaryotic genome annotation. *Bioinformatics*, *30*, 2068–2069. https://doi.org/10.1093/bioinformatics/btu153

Seemann, T. (2015). *snippy: fast bacterial variant calling from NGS reads.*

Serra, D. O., Richter, A. M., Klauck, G., Mika, F., & Hengge, R. (2013). Microanatomy at cellular resolution and spatial order of physiological differentiation in a bacterial biofilm. *MBio*, *4*. https://doi.org/10.1128/mBio.00103-13

Shafikhani, S. H., Mandic-Mulec, I., Strauch, M. A., Smith, I., & Leighton, T. (2002). Postexponential regulation of sin operon expression in Bacillus subtilis. *Journal of Bacteriology*, *184*, 564–571. https://doi.org/10.1128/JB.184.2.564-571.2002

Si, T., Li, B., Zhang, K., Xu, Y., Zhao, H., & Sweedler, J. V. (2016). Characterization of bacillus subtilis colony biofilms via mass spectrometry and fluorescence imaging. *Journal of Proteome Research*, *15*, 1955–1962. https://doi.org/10.1021/acs.jproteome.6b00127

Skinner, M. E., Uzilov, A. V., Stein, L. D., Mungall, C. J., & Holmes, I. H. (2009). JBrowse: A next-generation genome browser. *Genome Research*, *19*, 1630–1638. https://doi.org/10.1101/gr.094607.109

Srinivasan, S., Vladescu, I. D., Koehler, S. A., Wang, X., Mani, M., & Rubinstein, S. M. (2018). Matrix Production and Sporulation in Bacillus subtilis Biofilms Localize to Propagating Wave Fronts. *Biophysical Journal*, *114*, 1490–1498. https://doi.org/10.1016/j.bpj.2018.02.002

Staroń, A., Finkeisen, D. E., & Mascher, T. (2011). Peptide antibiotic sensing and detoxification modules of Bacillus subtilis. *Antimicrobial Agents and Chemotherapy*, *55*, 515–525. https://doi.org/10.1128/AAC.00352-10

Strauch, M. A., Perego, M., Burbulys, D., & Hoch, J. A. (1989). The transition state transcription regulator AbrB of Bacillus subtilis is autoregulated during vegetative growth. *Molecular Microbiology*, *3*, 1203–1209. https://doi.org/10.1111/j.1365-2958.1989.tb00270.x

Strauch, M. A., Spiegelman, G. B., Perego, M., Johnson, W. C., Burbulys, D., & Hoch, J. A. (1989). The transition state transcription regulator abrB of Bacillus subtilis is a DNA binding protein. *EMBO Journal*, *8*, 1615–1621. https://doi.org/10.1002/j.1460-2075.1989.tb03546.x

Strauch, M., Webb, V., Spiegelman, G., & Hoch, J. A. (1990). The SpoOA protein of Bacillus subtilis is a repressor of the abrB gene. *Proceedings of the National Academy of Sciences of the United States of America*, *87*, 1801–1805. https://doi.org/10.1073/pnas.87.5.1801

Trach, K., Burbulys, D., Strauch, M., Wu, J. J., Dhillon, N., Jonas, R., Hanstein, C., Kallio, P., Perego, M., Bird, T., Spiegelman, G., Fogher, C., & Hoch, J. A. (1991). Control of the initiation of sporulation in Bacillus subtilis by a phosphorelay. *Research in Microbiology*, *142*, 815–823. https://doi.org/10.1016/0923-2508(91)90060-N

van Gestel, J., Vlamakis, H., & Kolter, R. (2015). Division of Labor in Biofilms: the Ecology of Cell Differentiation. *Microbiology Spectrum*, *3*. https://doi.org/10.1128/microbiolspec.mb-0002-2014

Vlamakis, H., Aguilar, C., Losick, R., & Kolter, R. (2008). Control of cell fate by the formation of an architecturally complex bacterial community. *Genes and Development*, *22*(7), 945–953. https://doi.org/10.1101/gad.1645008

Wach, A. (1996). PCR-synthesis of marker cassettes with long flanking homology regions for gene disruptions in S. cerevisiae. *Yeast*, *12*, 259–265. https://doi.org/10.1002/(SICI)1097-0061(19960315)12:3<259::AID-YEA901>3.0.CO;2-C

Wang, X., Hao, M., & Wang, G. (2016). Numerical simulation of wrinkle morphology formation and the evolution of different Bacillus subtilis biofilms. *Water Science and Technology*, *73*, 527–534. https://doi.org/10.2166/wst.2015.486

Wick, R. R., Judd, L. M., Gorrie, C. L., & Holt, K. E. (2017). Unicycler: Resolving bacterial genome assemblies from short and long sequencing reads. *PLoS Computational Biology*, *13*. https://doi.org/10.1371/journal.pcbi.1005595

Wüpping, K. L. , K. J.-P. , S. J. , D. K. (2024, June 2). MALDI-2 Mass Spectrometry Imaging of Peptide Toxins, Lipopeptides and Lipids in Thin Sections of Bacillus subtilis Biofilms. *72nd ASMS Conference on Mass Spectrometry and Allied Topics*.

Yannarell, S. M., Beaudoin, E. S., Talley, H. S., Schoenborn, A. A., Orr, G., Anderton, C. R., Chrisler, W. B., & Shank, E. A. (2023). Extensive cellular multi-tasking within Bacillus subtilis biofilms . *MSystems*. https://doi.org/10.1128/msystems.00891-22

Zhu, X., Xu, T., Peng, C., & Wu, S. (2022). Advances in MALDI Mass Spectrometry Imaging Single Cell and Tissues. In *Frontiers in Chemistry* (Vol. 9). Frontiers Media S.A. https://doi.org/10.3389/fchem.2021.782432

Supplemental data

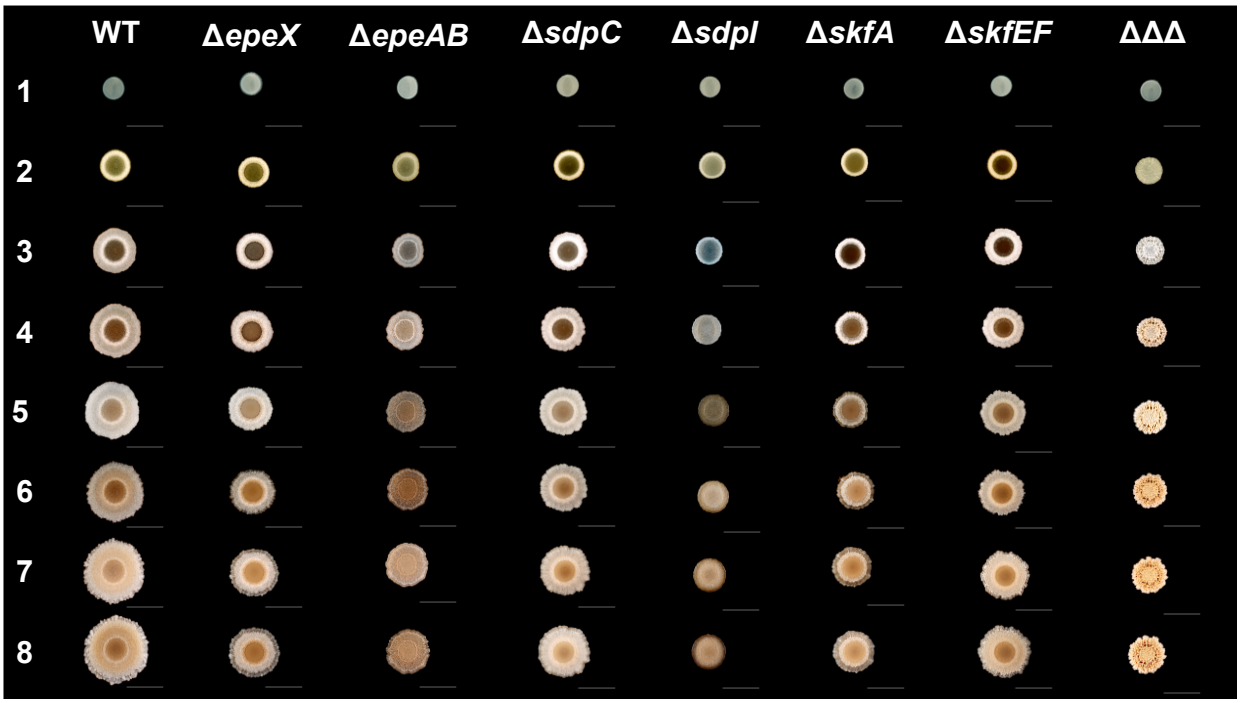

Fig. S1 **Growth of *B.subtilis* colonies on MSgg agar plates over 8 days**. Genotypes of the strains are written above, numbers on the left indicate the day of growth. Scale bar indicates 1cm.

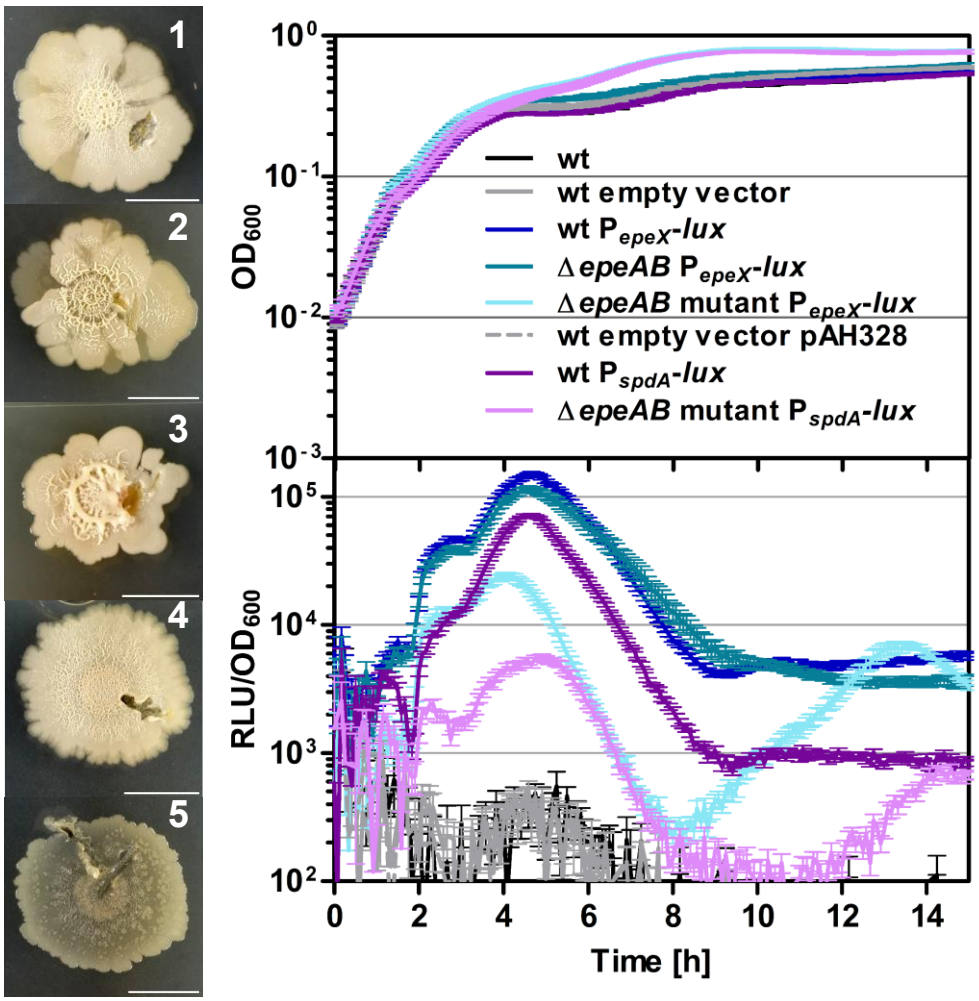

Fig. S2 **Left: Δ*epeAB* flare mutants 1-5 grown on MSgg agar (day 12 is shown). Right: Growth curve (top) and correlating relative luminescence (bottom) signal over time.** Cultures were grown in DSM medium. Color code for each strain is stated within the graph of the growth curve. P*empty*-lux is herein referred to as "empty vector (pAH328)". Scale bar indicates 1 cm. Error bars indicate standard error of the mean (SEM).

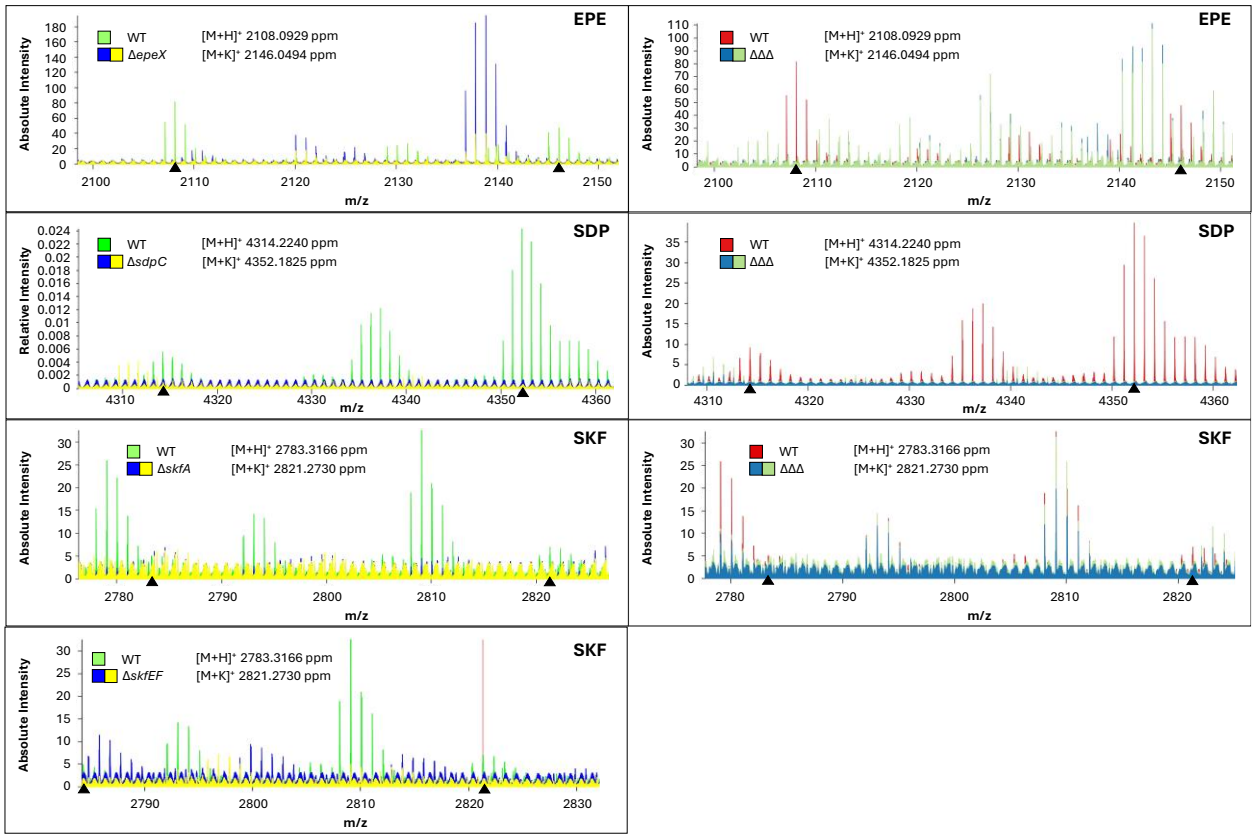

Fig. S3 **MALDI-MSI mass spectra**. Spectra of WT measurements as well as mutant measurements in duplicates are shown in absolute intensity values (y axis). Color code for each strain is shown within the graph. X axis shows mass-to-charge ratio with values representing $[M+H]^+$ and $[M+K]^+$ ion adducts of the respective toxins, indicated by a black triangle.

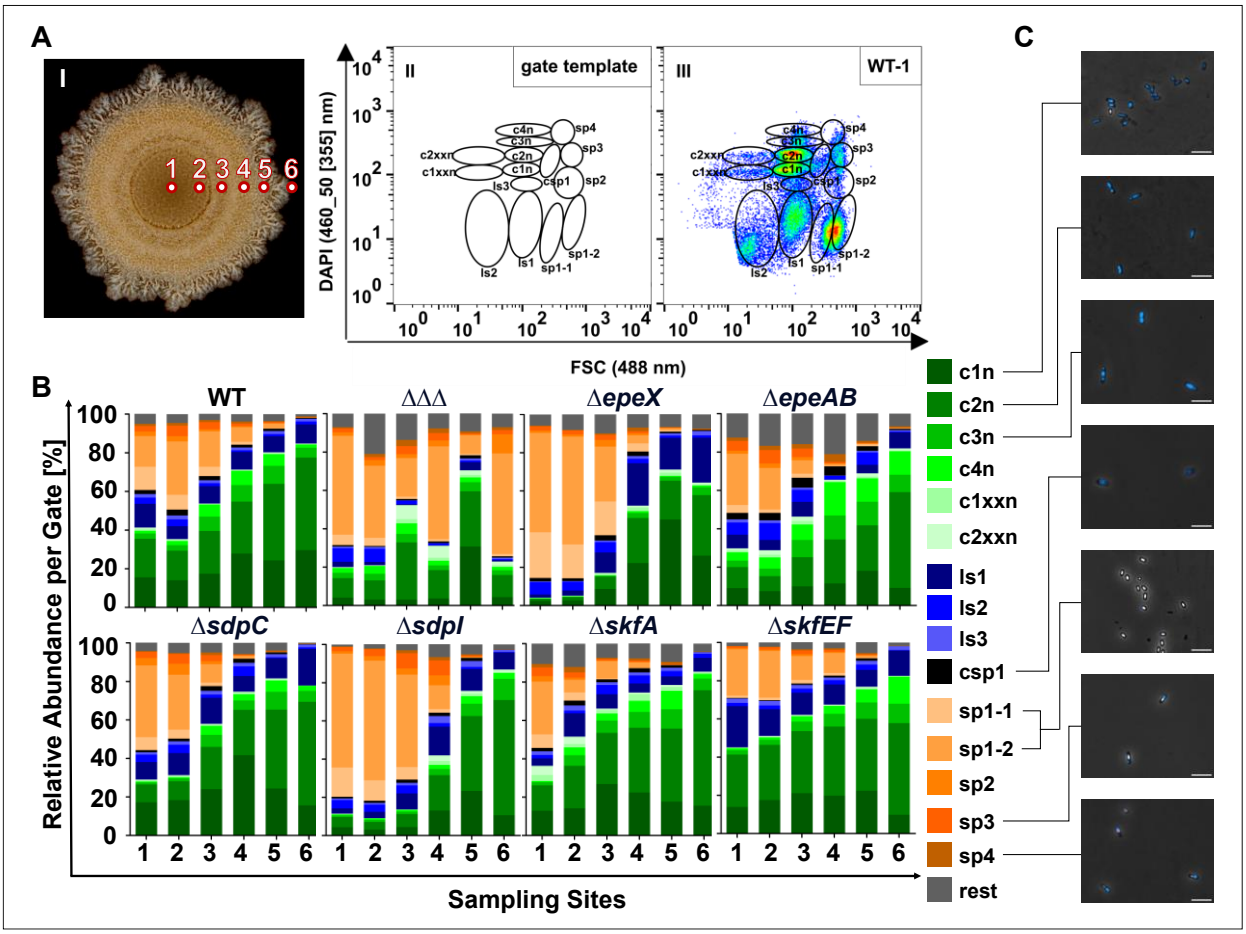

Fig. S4 **Distribution of cell types across *B. subtilis* colonies regarding cannibalism after DAPI staining.** [A] Sampling sites across an exemplary WT colony are shown on the left. On the right, gate templates for analysis and sorting are depicted, as well as an exemplary dataset of flow cytometric measurement of cells present in sampling site 1 of the WT. DAPI signal is plotted against forward scatter (FSC). [B] Overview of flow cytometric analysis results are summarized in bar graphs for each strain, where the relative abundance of cells per gate is plotted against sampling sites. c1n – c2xxn indicate vegetative cells, and ls1 – ls3 indicate less stained cells, meaning that they do not take up DAPI easily. Csp1, sp1-1 – sp4 represent different spore types. [C] Microscopy images of sorted cells from the WT representing some of the analyzed occurring cell types. Scale bar indicates 5 µm.

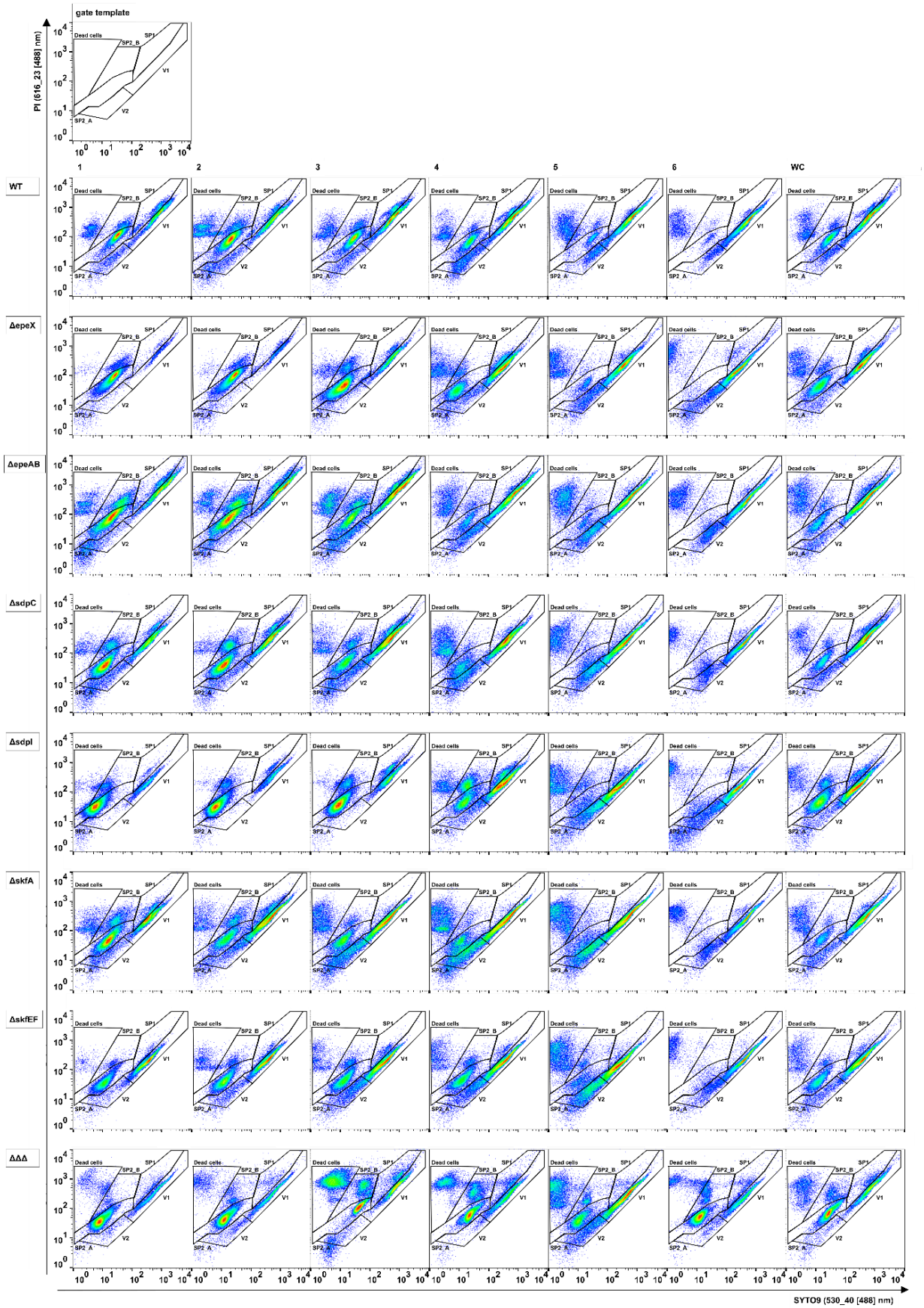

Fig. S5 **Overview of flow cytometric results for SYTO9 PI staining.** Top left shows the gate template. Datasets for each strain are shown in a row, starting with sampling site 1-6, followed by the data obtained for the whole colony (WC). 2D plots depict SYTO9 against PI data [rel. FI].

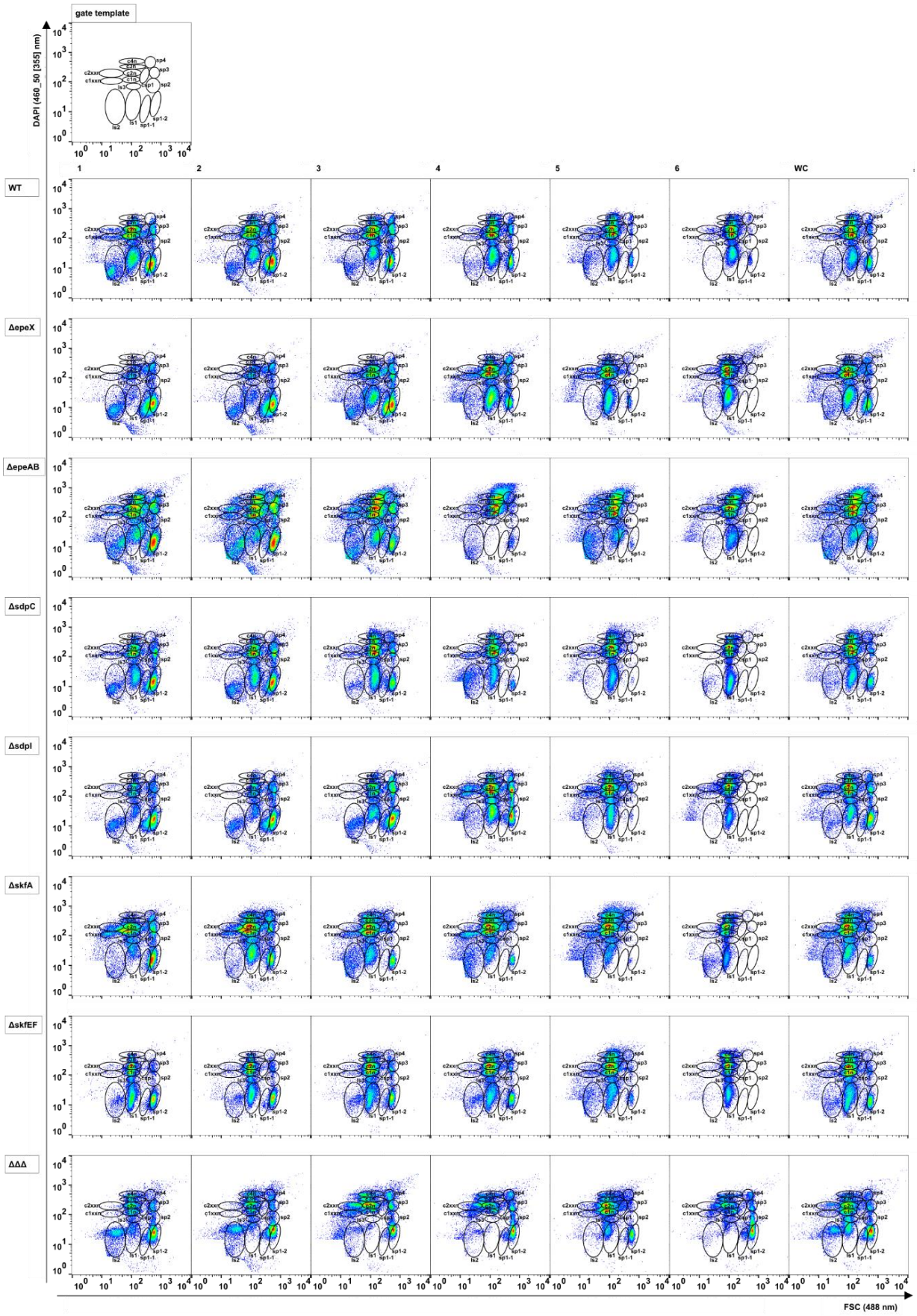

Fig. S6 **Overview of flow cytometric results for DAPI staining.** Top left shows the gate template. Datasets for each strain are shown in a row, starting with sampling site 1-6, followed by the data obtained for the whole colony (WC). 2D plots depict FSC against DAPI data [rel. FI].